Electronic Supplementary Material (ESI) for Journal of Materials Chemistry A.

Electronic Supplementary Information

Perovskite $KNi_{0.1}Co_{0.9}F_3$ as a pseudocapacitive conversion anode for high-performance nonaqueous Li-ion capacitors and dual-ion batteries

Qilei Xu, **Rui Ding**,* Wei Shi, Danfeng Ying, Yongfa Huang, Tong Yan, Ping Gao, Xiujuan Sun and Enhui Liu

Key Laboratory of Environmentally Friendly Chemistry and Applications of Ministry of Education, College of Chemistry, Xiangtan University, Hunan 411105, P.R. China

* E-mails: drm8122@163.com; drm8122@xtu.edu.cn (R. Ding);

Tel: +86 731 58292202; Fax: +86 731 58292251

Table of contents

Fig. S1 A picture of KNCF samples (Ni/Co=1-0~0-1).

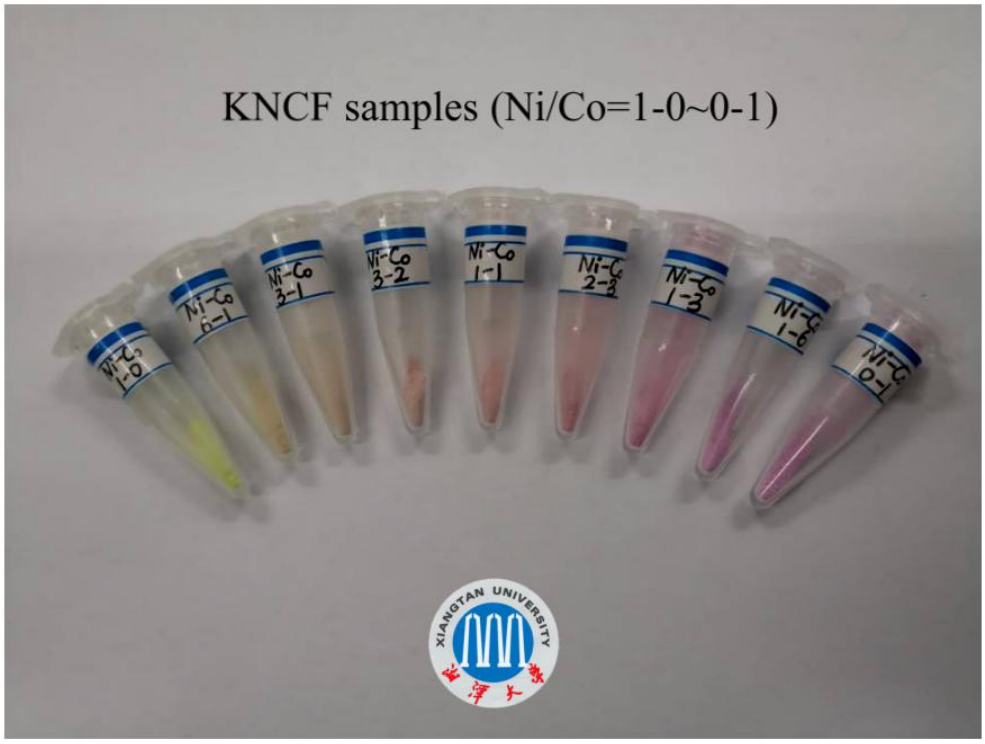

Fig. S2 The crystal structures of perovslite KMF_3 and detailed crystalline parameters for $KNiF_3$ and $KCoF_3$.

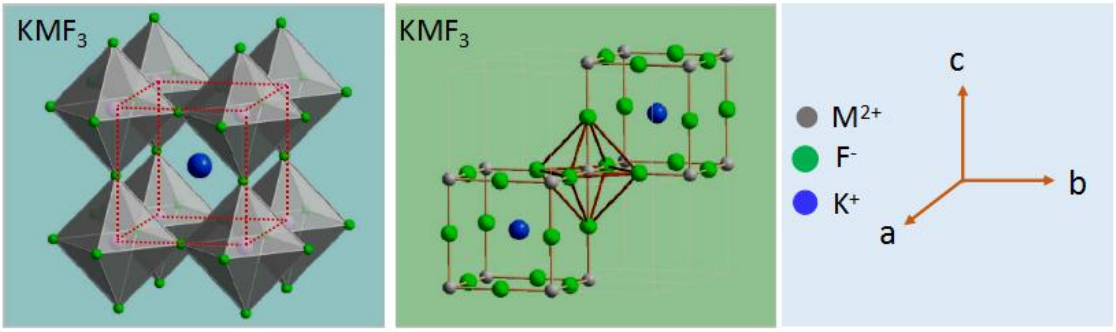

Sample	ICDD-PDF	Cyrstal system	Space group	Cell (a x b x c) / Å^3
$KNiF_3$	21-1002	Cubic	Pm3m	4.013 x 4.013 x 4.013
$KCoF_3$	18-1006	Cubic	Pm3m	4.071 x 4.071 x 4.071

Fig. S3 SEM-TEM images of KNCF (1-6) Samples.

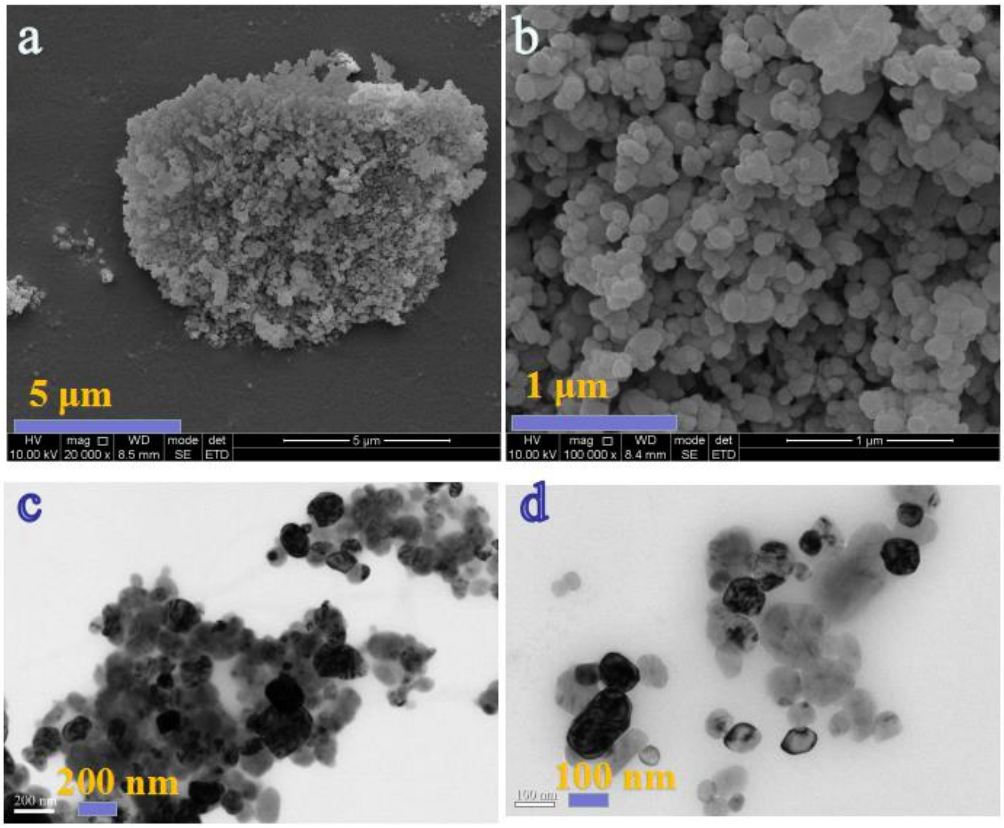

Fig. S4 Element mapping of KNCF(1-6) samples from TEM images.

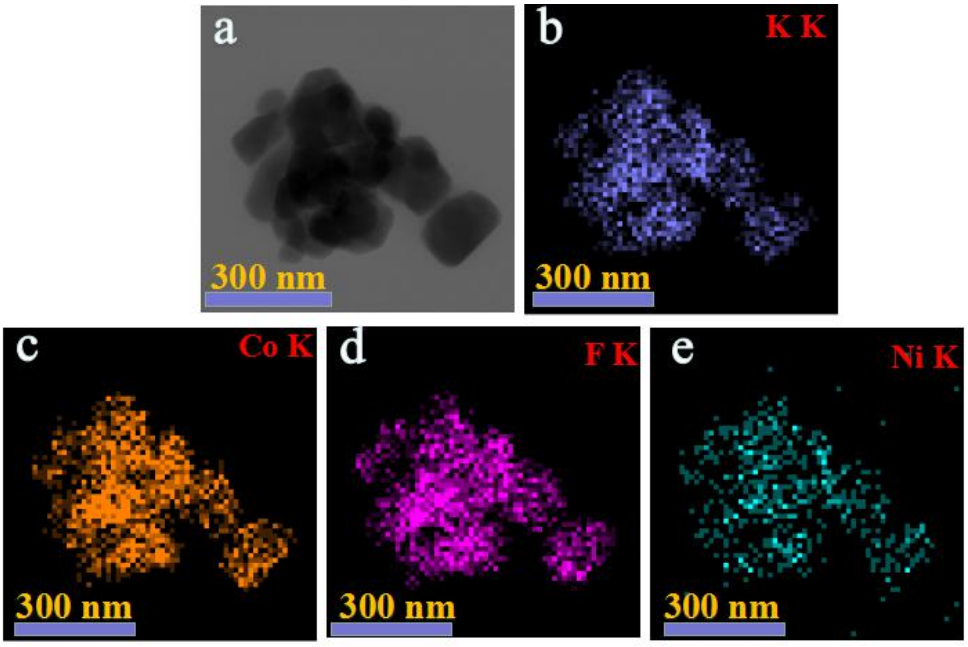

Fig. S5 XPS spectra of KNCF (1-6) electrode in pristine, charged-3 V and discharged-0.01 V states of the 3rd CV (0.3 mV s^{-1}) cycle with A electrolytes.

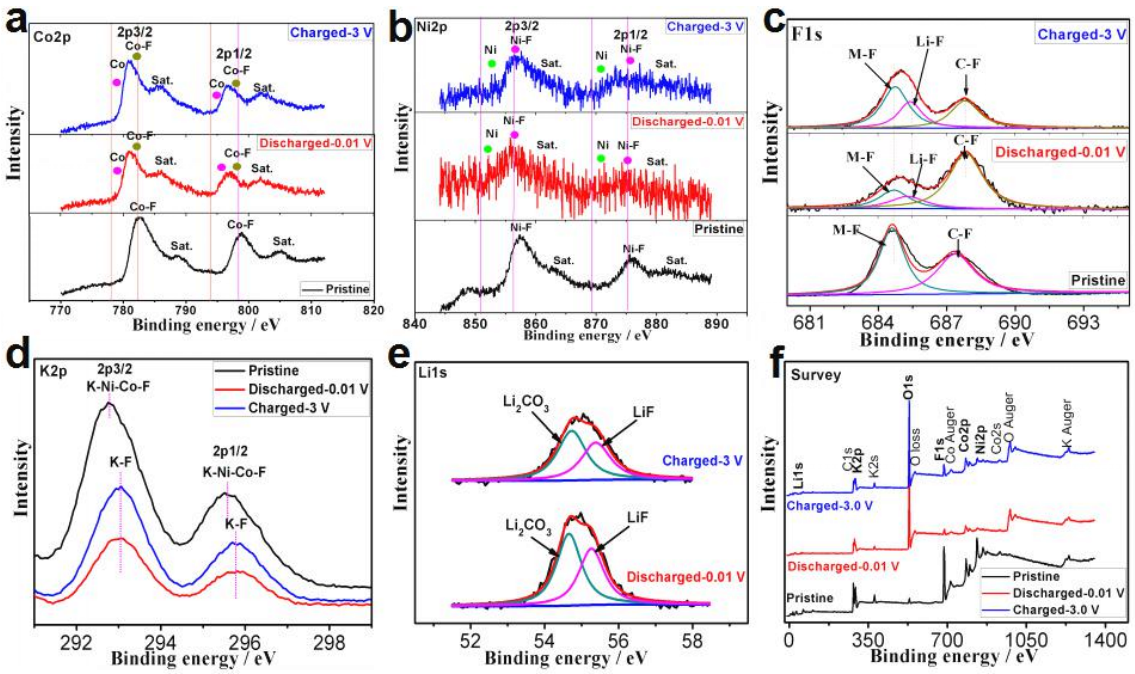

Fig. S6 TEM and SAED patterns for the KNCF (1-6) electrode incharged-3 V and discharged-0.01 V states of the 3rd CV (0.3 mV s^{-1}) cycle with A electrolytes (a); Crystalline structure information of Ni, Co, NiF_2, CoF_2, KF, LiF and Li_2CO_3phases (b).

(a)

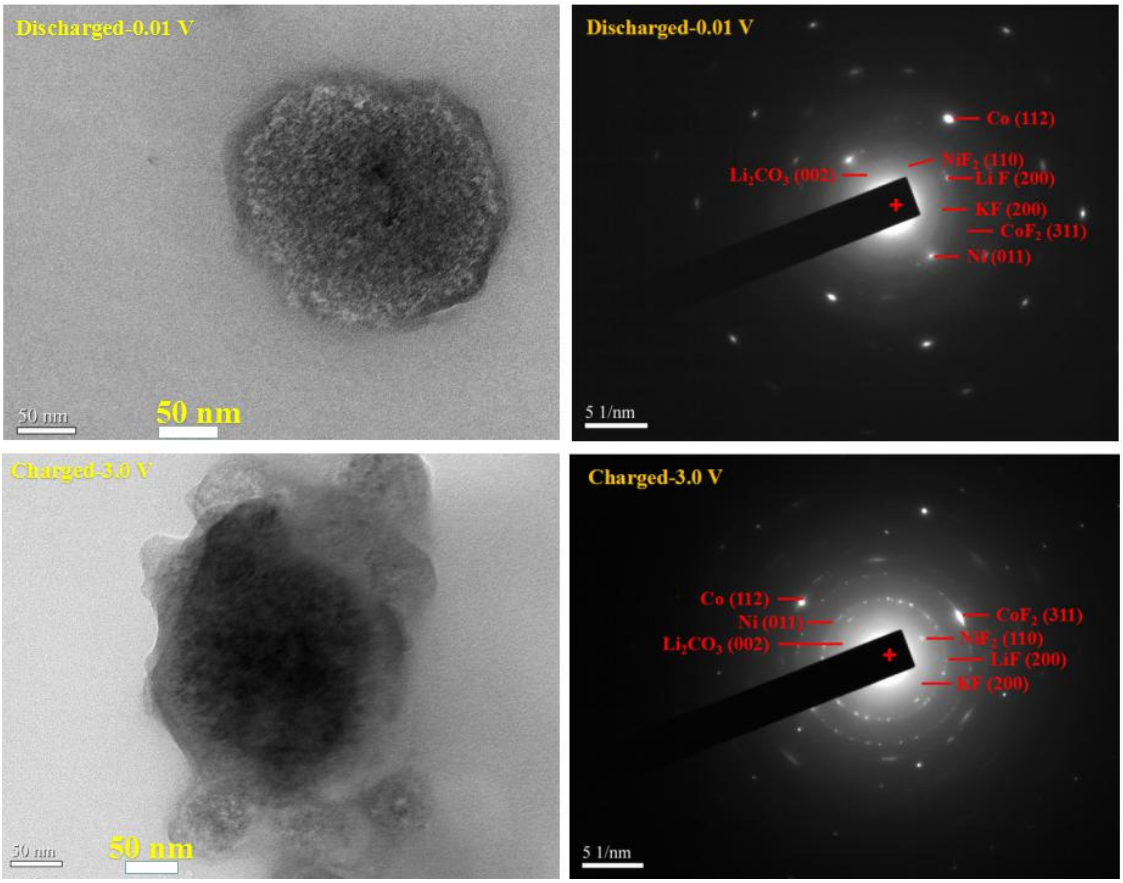

(b)

Phases	PDF Card	Crystal system	Space group	Cell (a x b x c) / Å^3
Ni	45-1027	Hexagonal	P63/mmc	2.651 X 2.651 X 4.343
Co	05-0727	Hexagonal	P63/mmc	2.503 X 2.503 X 4.061
NiF_2	24-0792	Tetragonal	P42/mnm	4.651 X 4.651 X 3.084
CoF_2	38-0883	Cubic	Pa3	4.958 X 4.958 X 4.958
LiF	45-1460	Cubic	Fm-3m	4.027 X 4.027 X 4.027
KF	36-1458	Cubic	Fm-3m	5.348 X 5.348 X 5.348
Li_2CO_3	22-1141	Monoclinic	C2/c(15)	8.359 x 4.977 x 6.194

Fig. S7 Ex-situ XRD patterns of KNCF (1-6) electrode in pristine, the 1st discharge (Dis)/charge (Ch) (0.1 A g^{-1}) processes with A electrolytes.

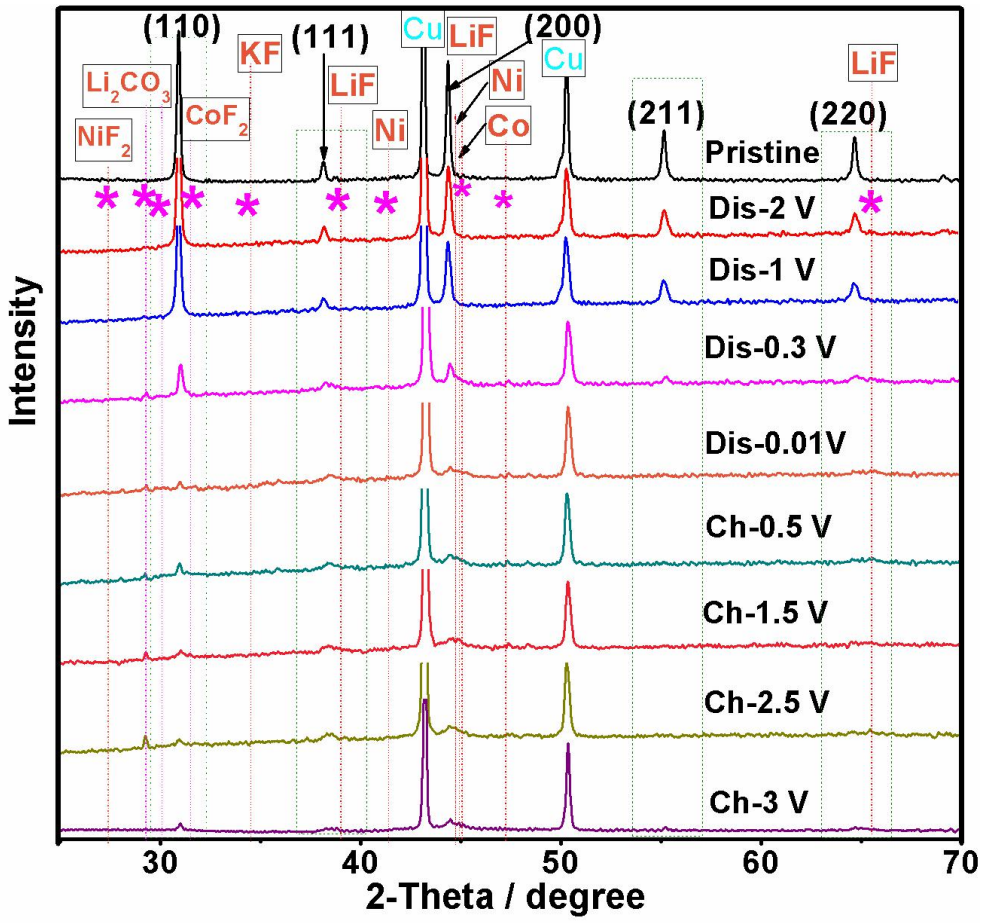

Fig. S8 Schematics of possible reaction mechanisms for KMF_3 (M=Ni, Co) electrode during the discharging/charging processes under the first two cycles.

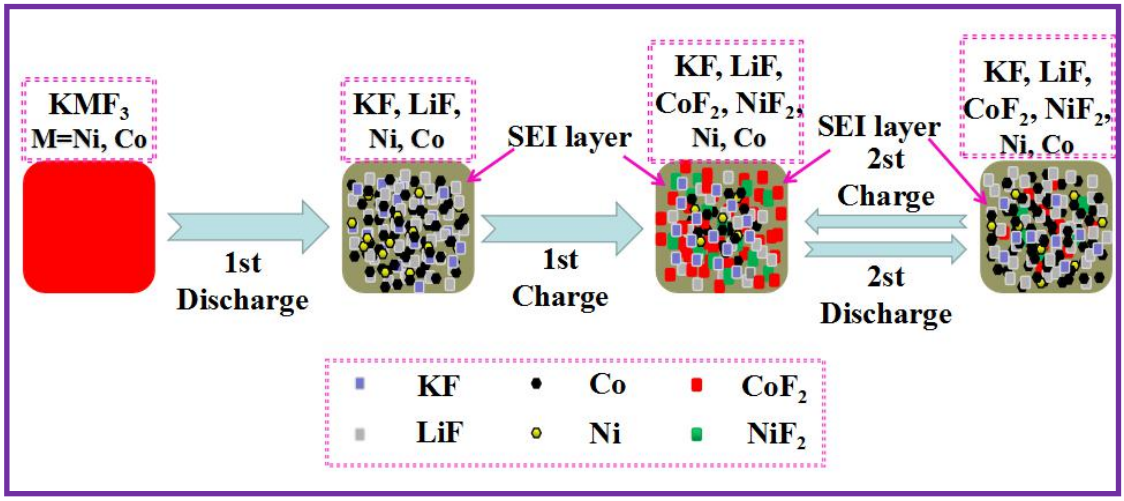

Fig. S9 CV plots of the first three cycles of KNCF electrodes at 0.3 mV s^{-1} with A electrolytes.

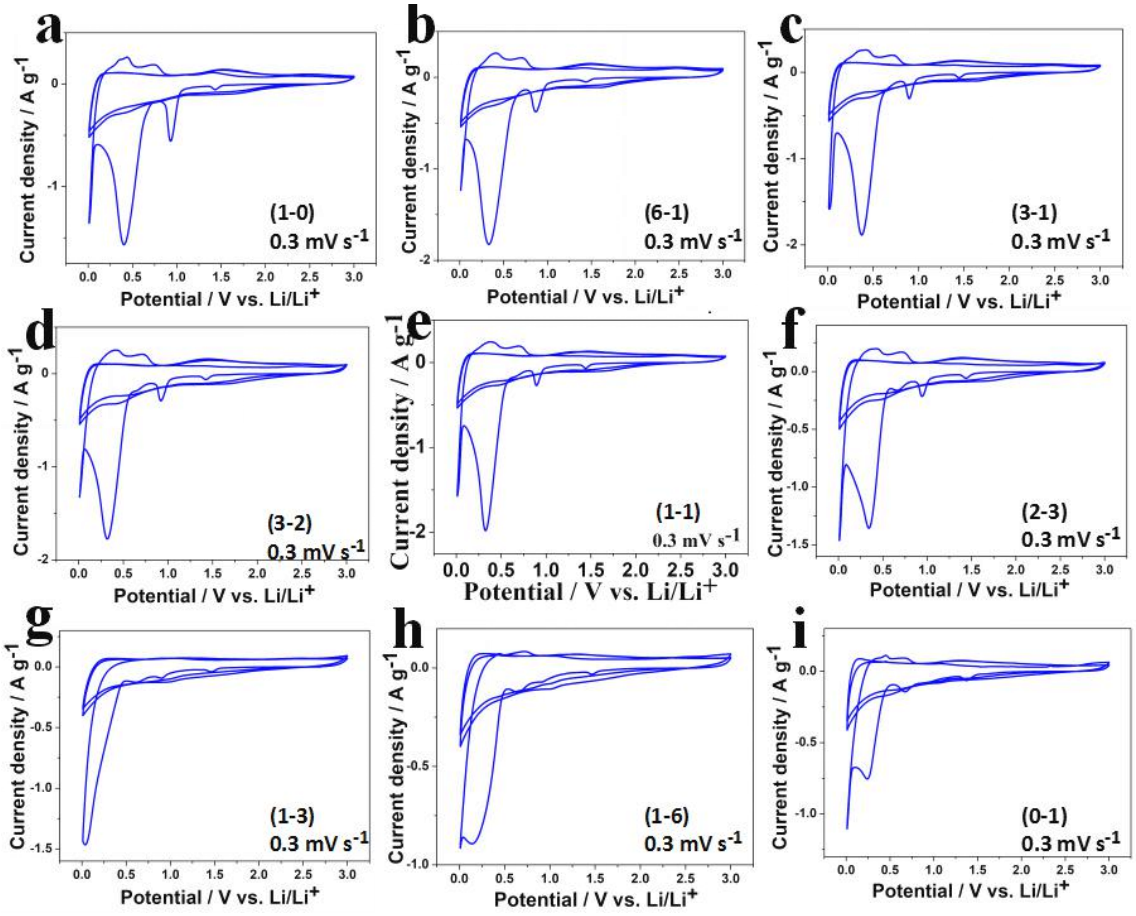

Fig. S10 GCD curves-the first five cycles of KNCF electrodes at 0.1 A g^{-1} with A electrolytes.

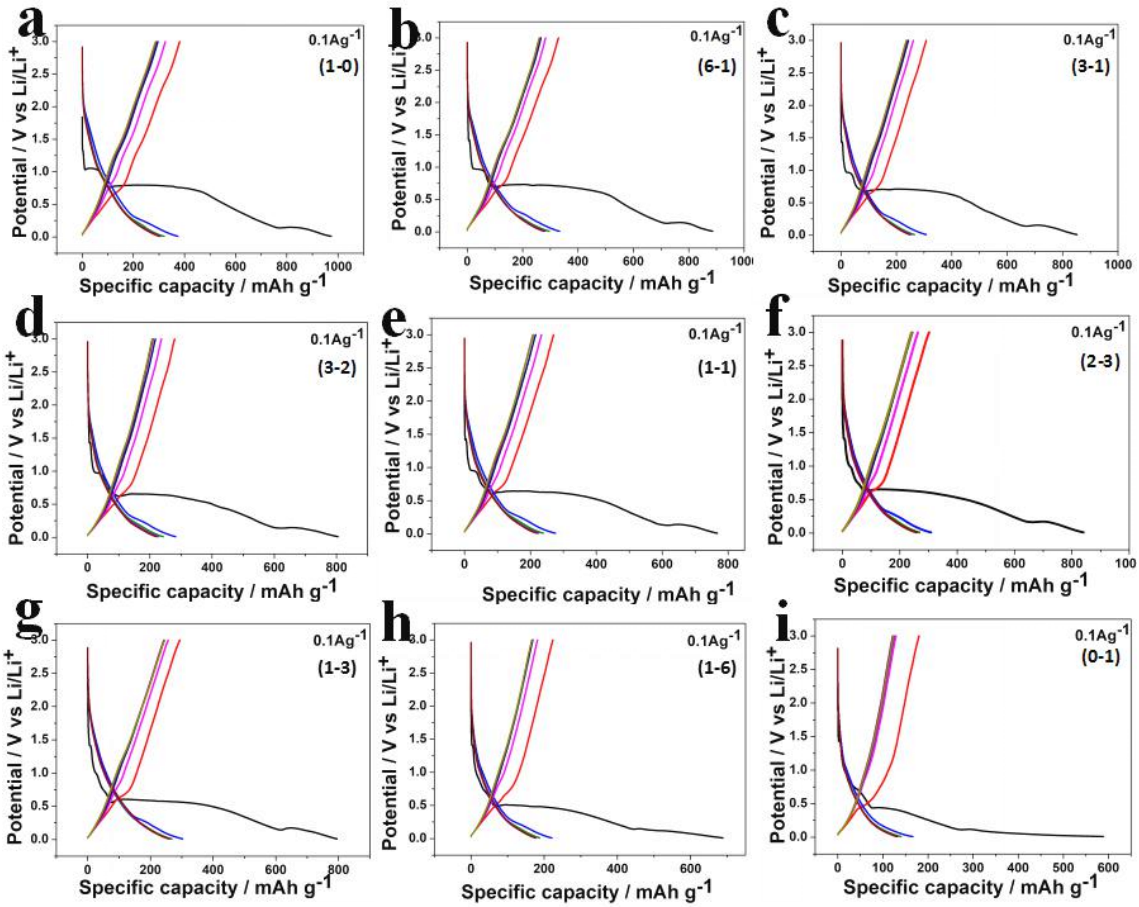

Fig. S11 GCD curves of KNCF electrodes at 0.1~3.2 A g^{-1} with A electrolytes.

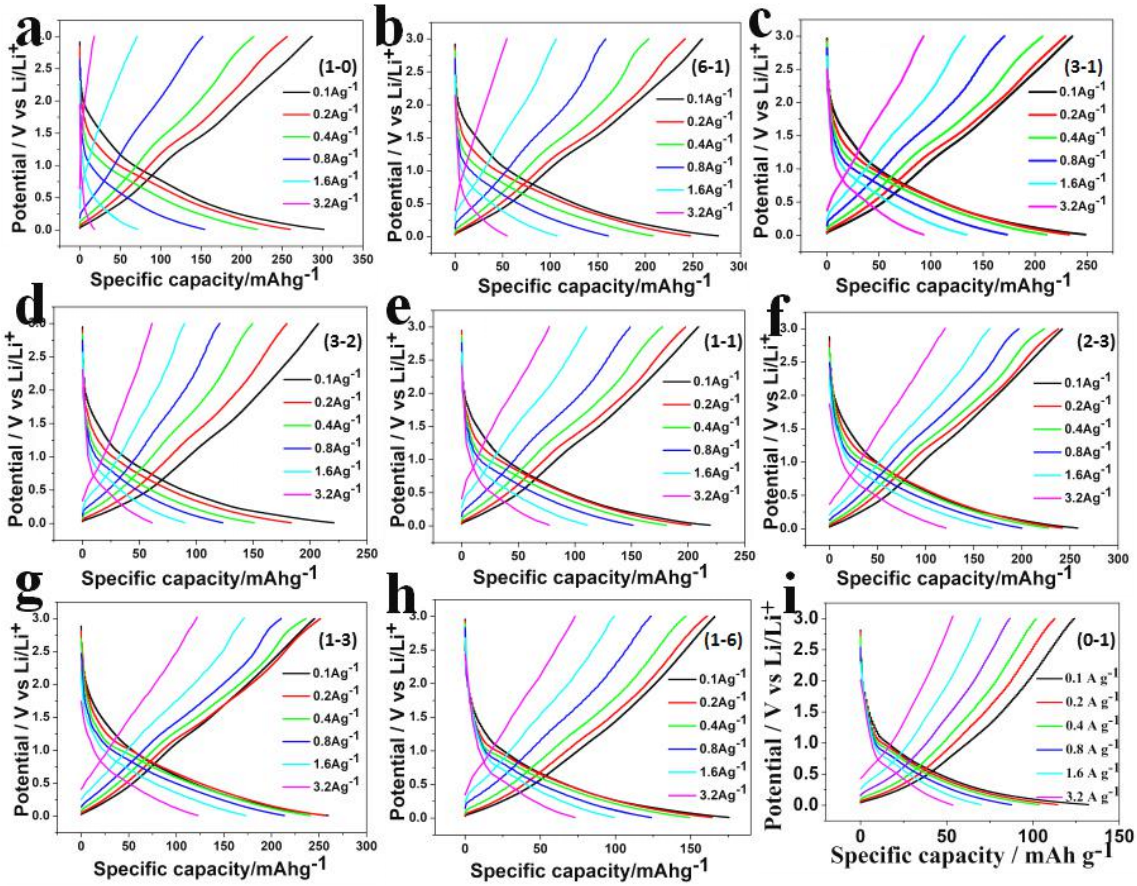

Fig. S12 Rate performance and Coulombic efficiency of KNCF electrodes at 0.1~3.2~0.1 A g^{-1} with A electrolytes.

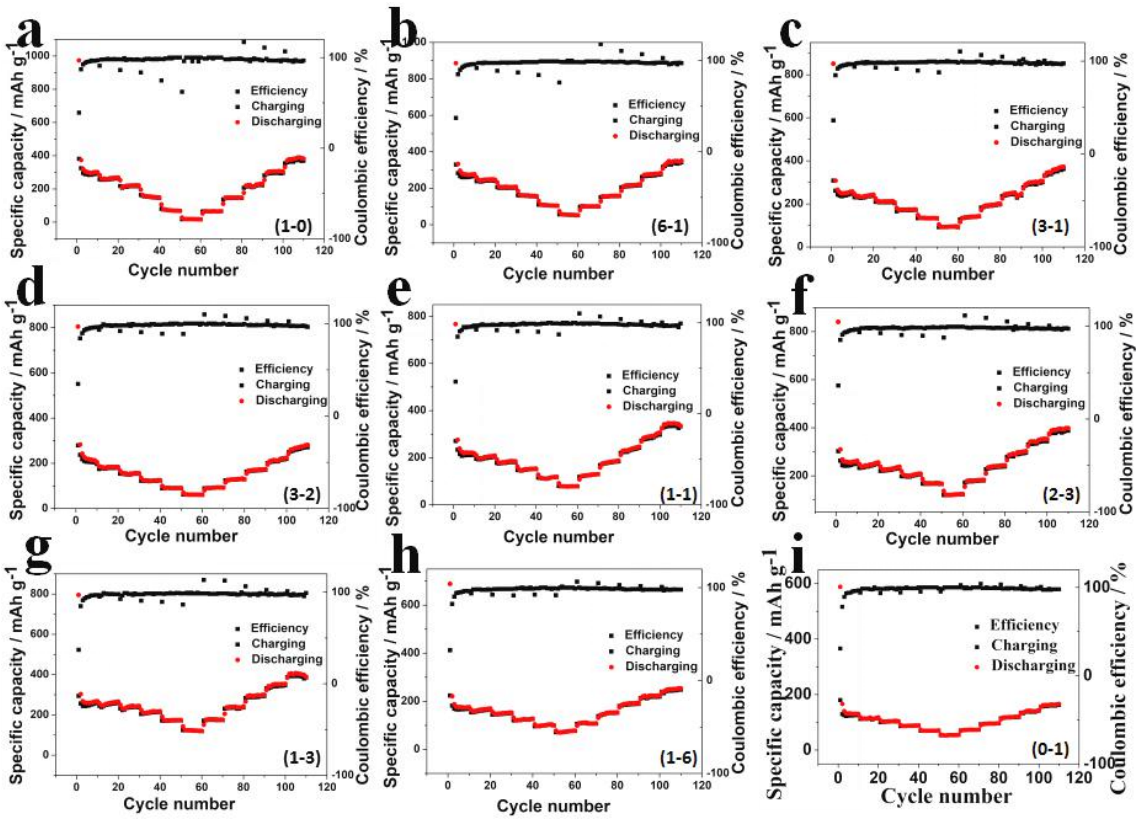

Fig. S13 Cycling stability and Coulombic efficiency of KNCF electrodes at 1 A g^{-1} for 1000 cycles with A electrolytes.

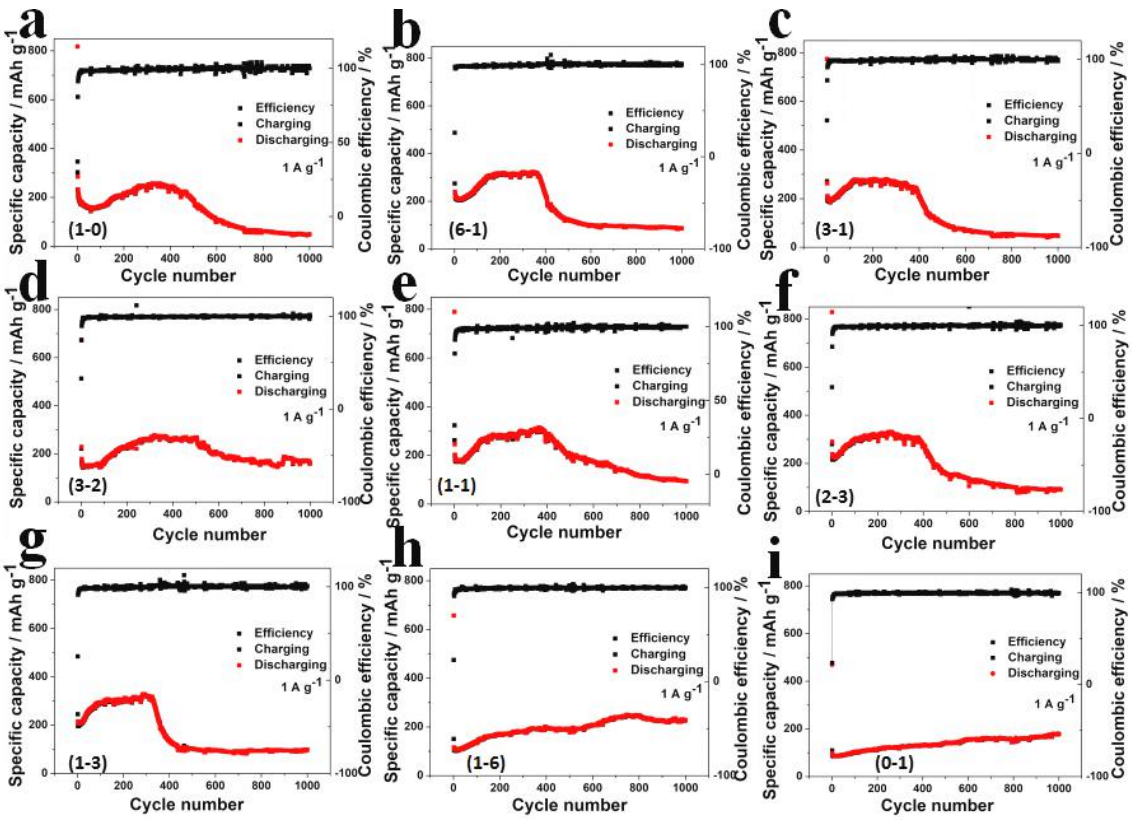

Fig. S14 Performance of AC electrode with A electrolytes.

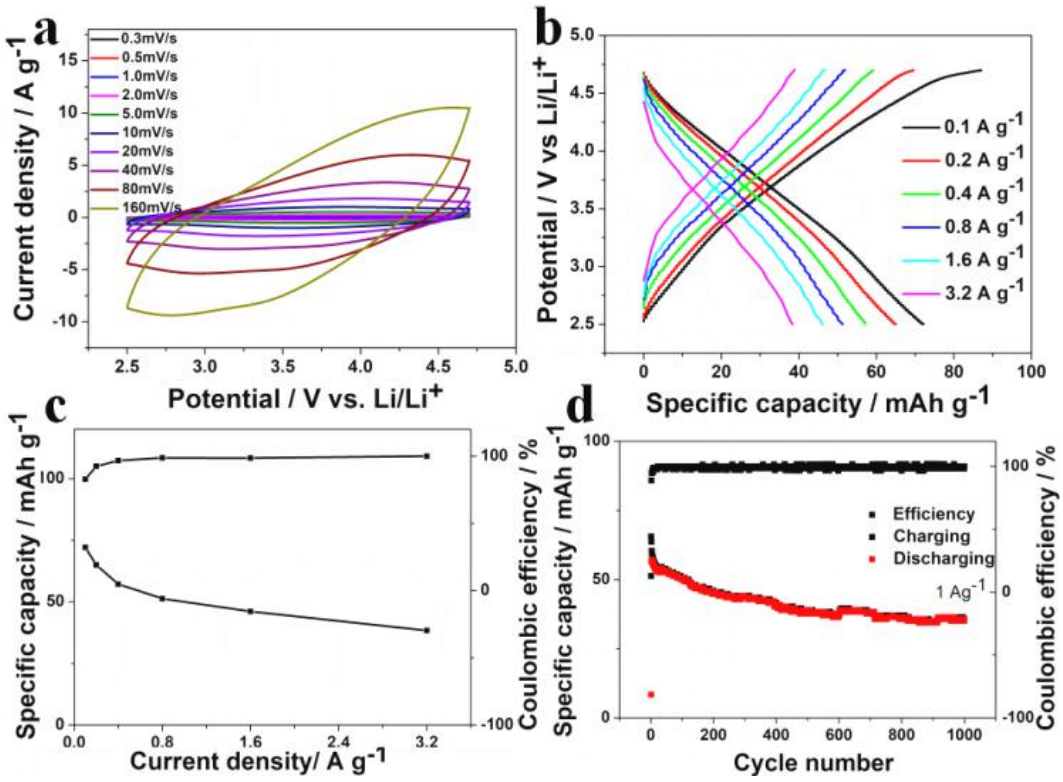

Fig. S15 CV windows of KNCF//AC LICs (Ni/Co=1-0~0-1) at 50 mV s^{-1} with A electrolytes.

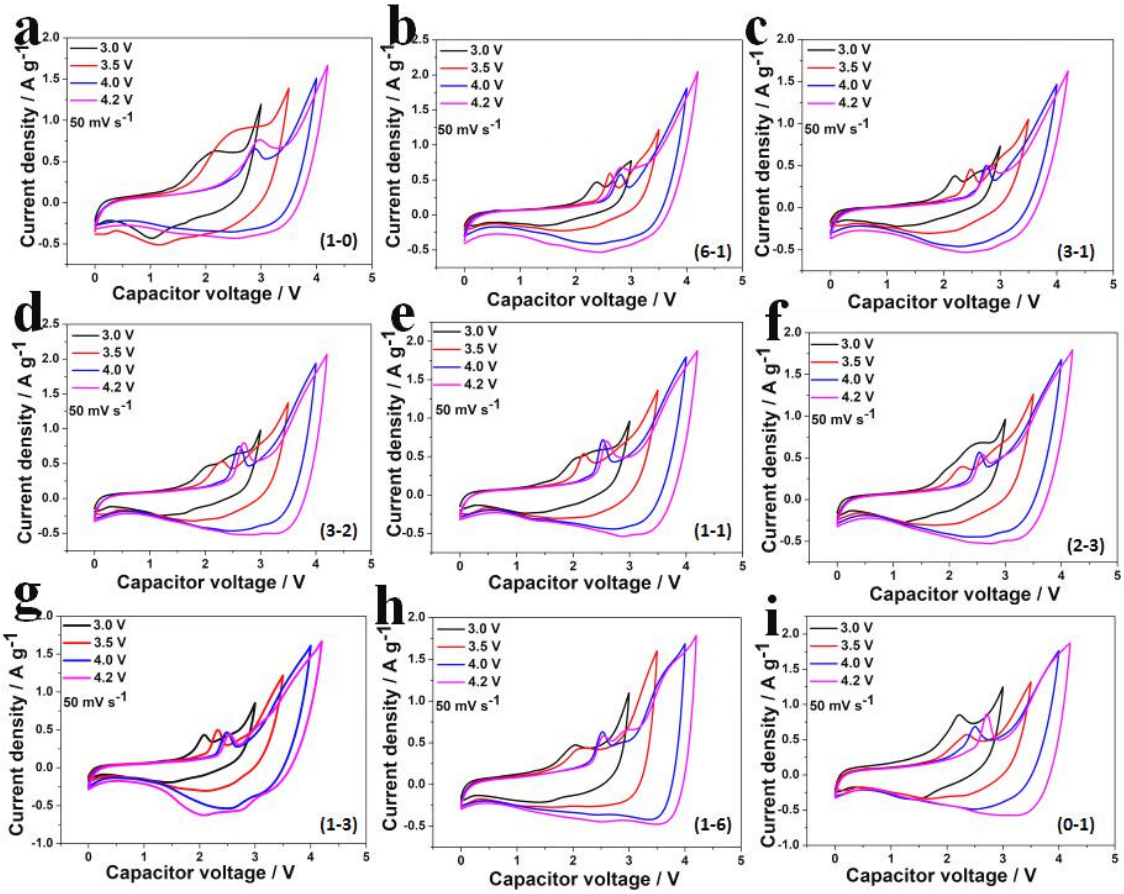

Fig. S16 CV plots of KNCF//AC LICs (Ni/Co=1-0~0-1) at 10~160 mV s^{-1} with A electrolytes.

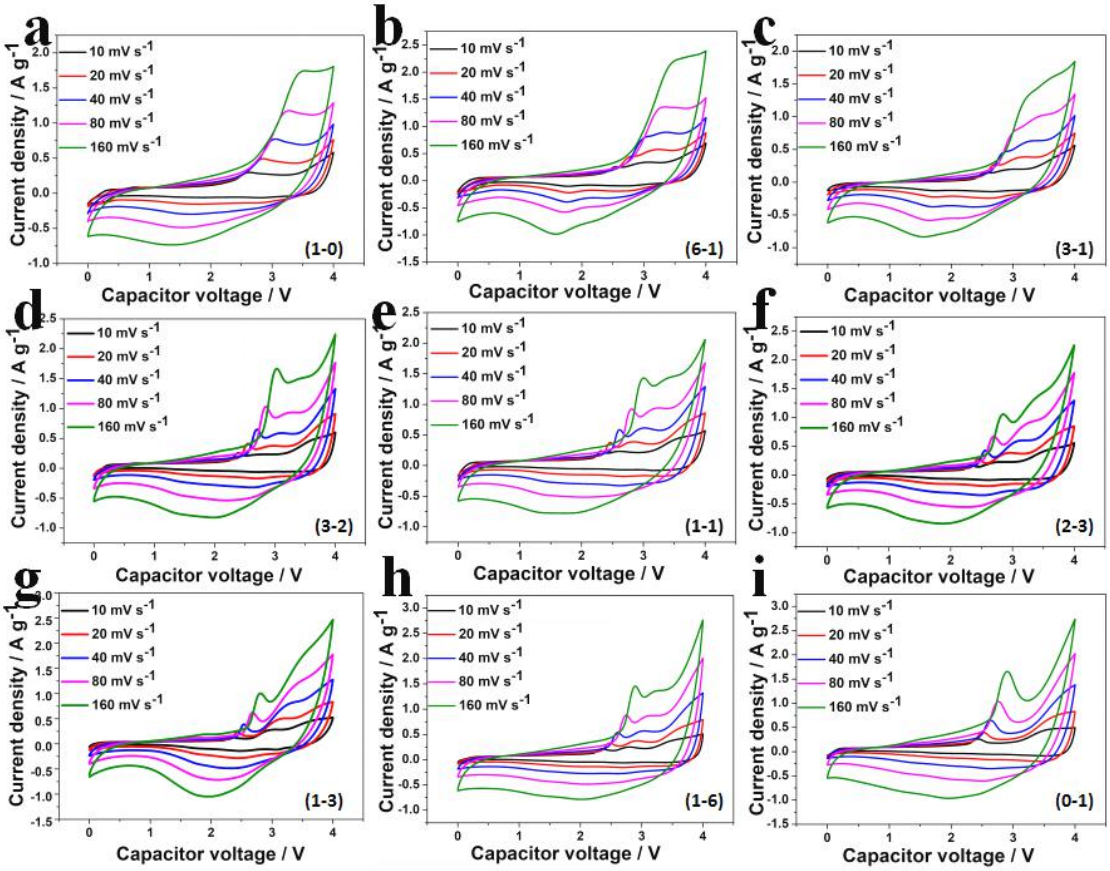

Fig. S17 GCD curves of KNCF//AC LICs (Ni:Co=1-0~0-1) at 0.5~8 A g^{-1} with A electrolytes.

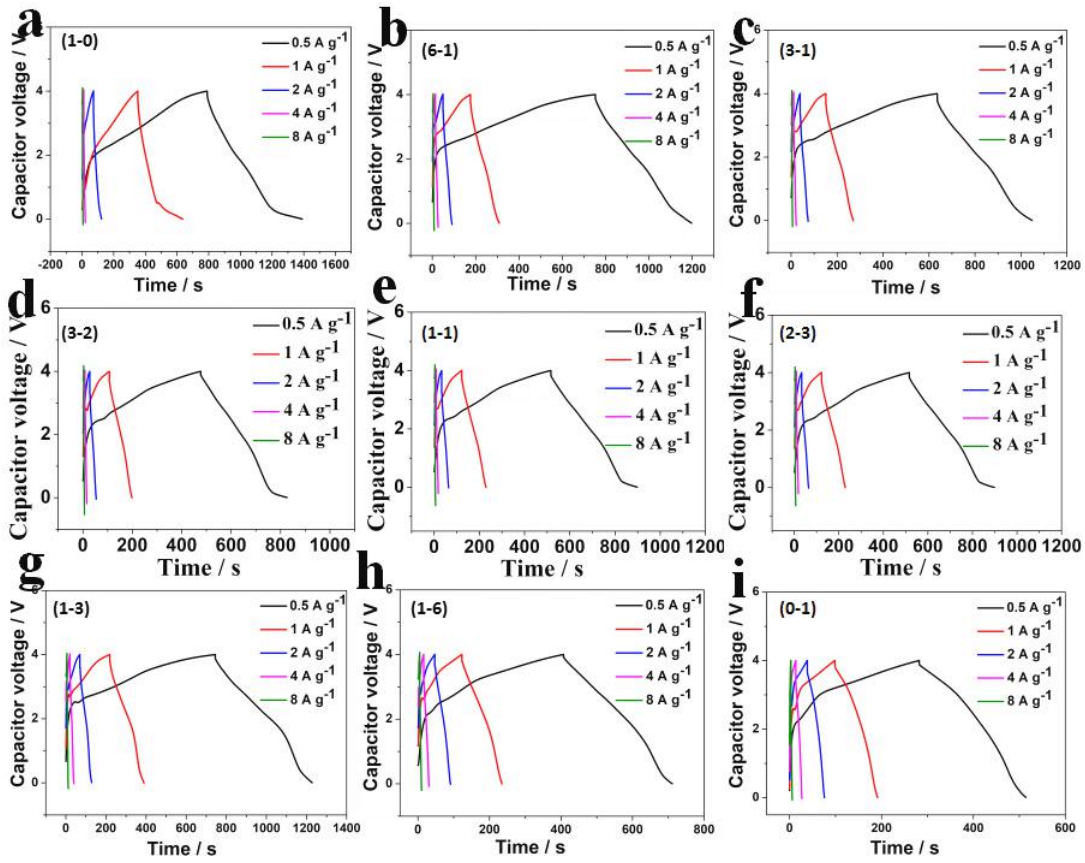

Fig. S18 Cycling stability and Coulombic efficiency of KNCF//AC LICs (Ni:Co=1-0~0-1) at 1 A g^{-1} with A electrolytes.

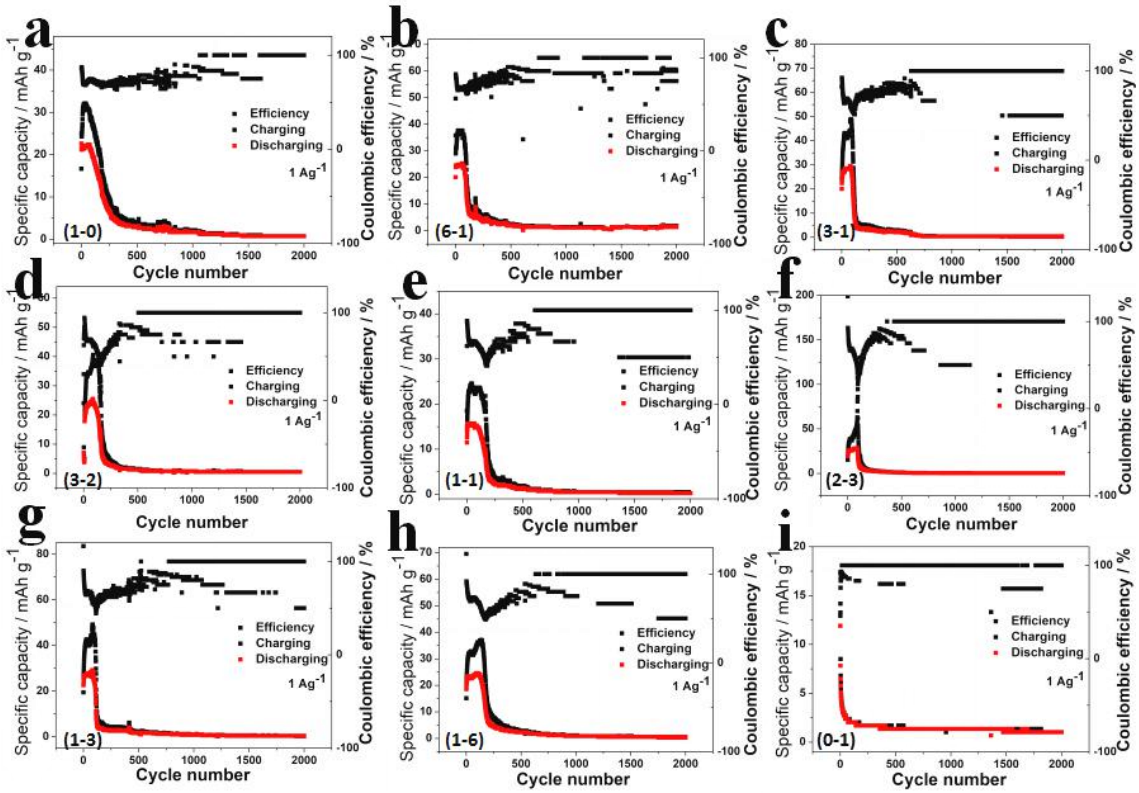

Fig. S19 GCD curves of KNCF(2-3) electrode at the precharged current densities of 0.1-2 A g^{-1} with A electrolytes.

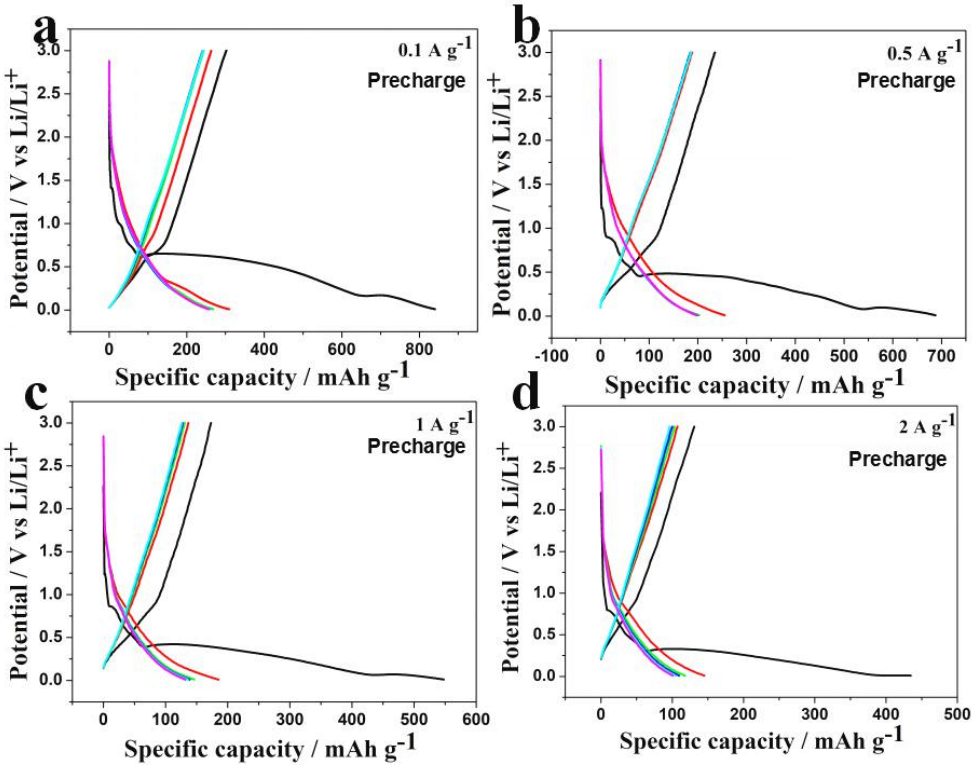

Fig. S20 CV windows of KNCF (2-3)//AC LICs at 50 mV s^{-1} with the anode precharged at 0.1-2 A g^{-1} and A electrolytes.

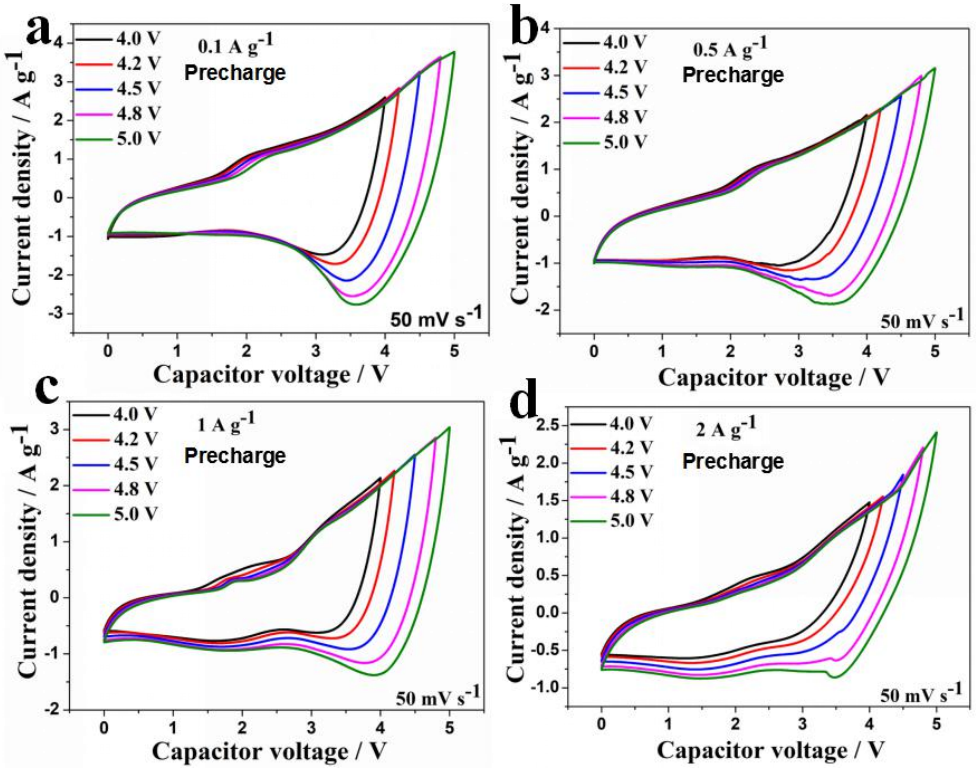

Fig. S21 GCD curves of KNCF (2-3)//AC LICs at 0.5-16 A g^{-1} with the anode precharged at 0.1-2 A g^{-1} and A electrolytes.

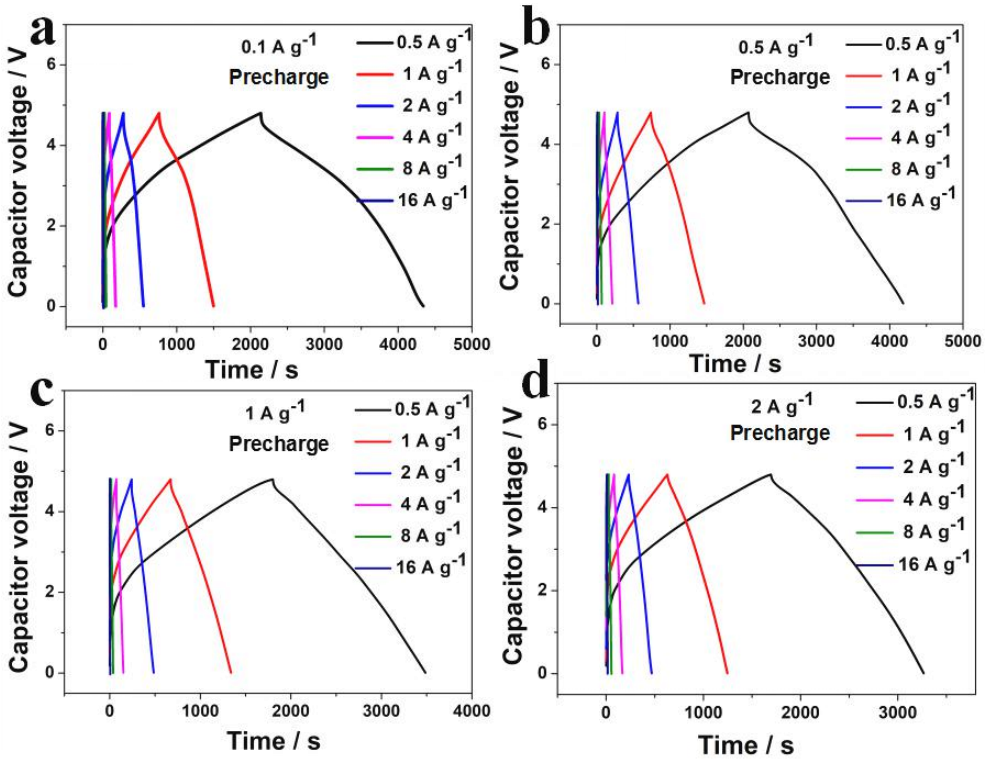

Fig. S22 Cycling stability and Coulombic efficiency of KNCF (2-3)//AC LICs at 5 A g^{-1} with the anode precharged at 0.1-2 A g^{-1} and A electrolytes.

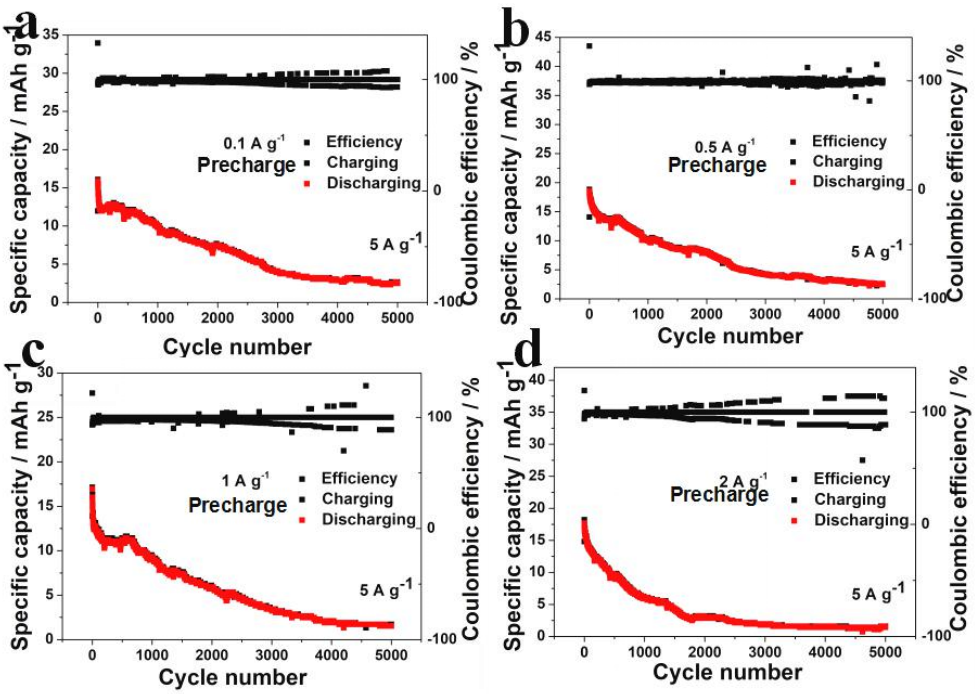

Fig. S23 CV windows of KNCF//AC LICs (Ni:Co=1-0, 2-3, 1-6, 0-1) at 30 mV s^{-1} with the anode precharged at 0.5 A g^{-1} and A electrolytes.

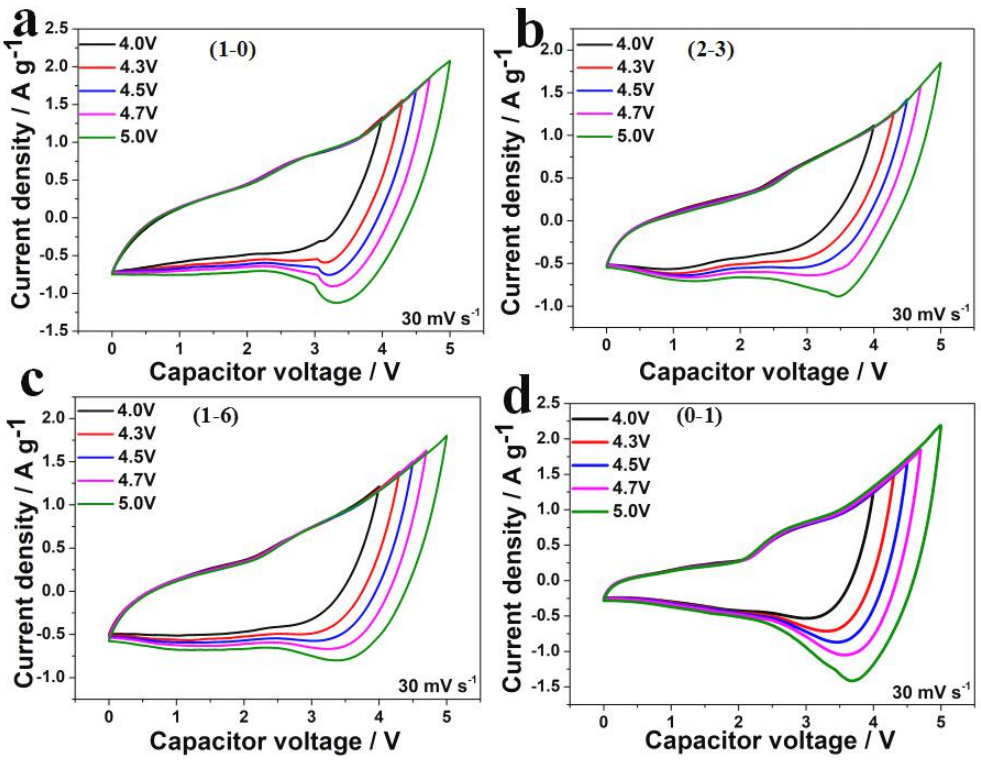

Fig. S24 CV plots of 4 V-KNCF//AC LICs (Ni:Co=1-0, 2-3, 1-6, 0-1) at 10-160 mV s^{-1} with the anode precharged at 0.5 A g^{-1} and A electrolytes.

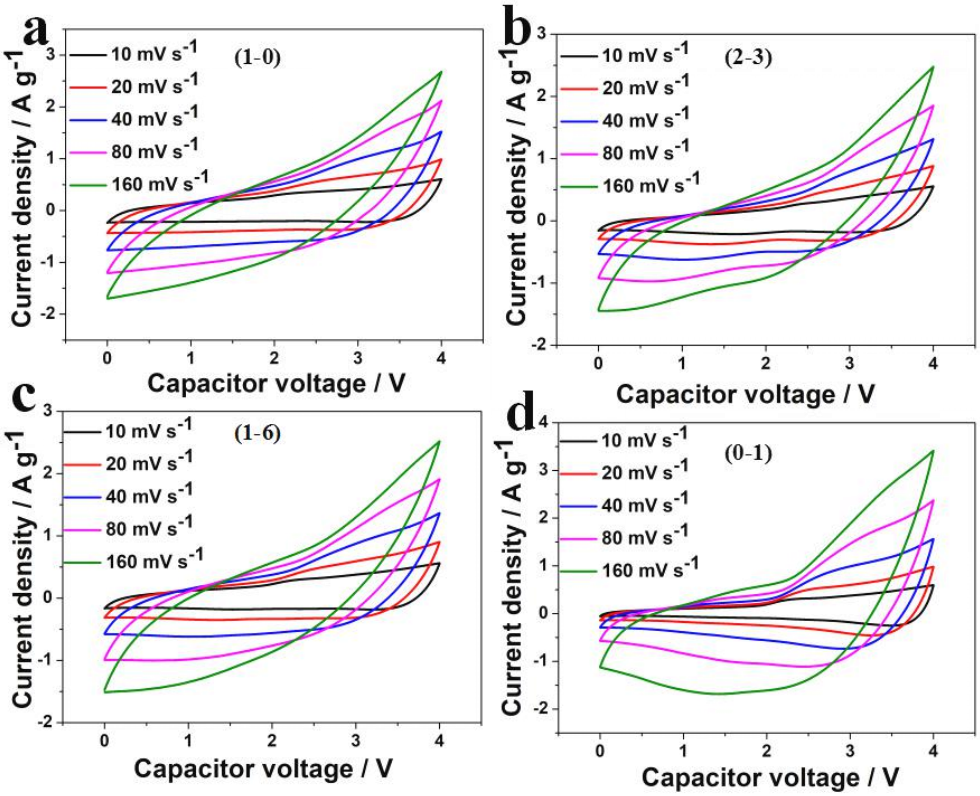

Fig. S25 GCD curves of 4 V-KNCF//AC LICs (Ni:Co=1-0, 2-3, 1-6, 0-1) at 0.5-16 A g^{-1} with the anode precharged at 0.5 A g^{-1} and A electrolytes.

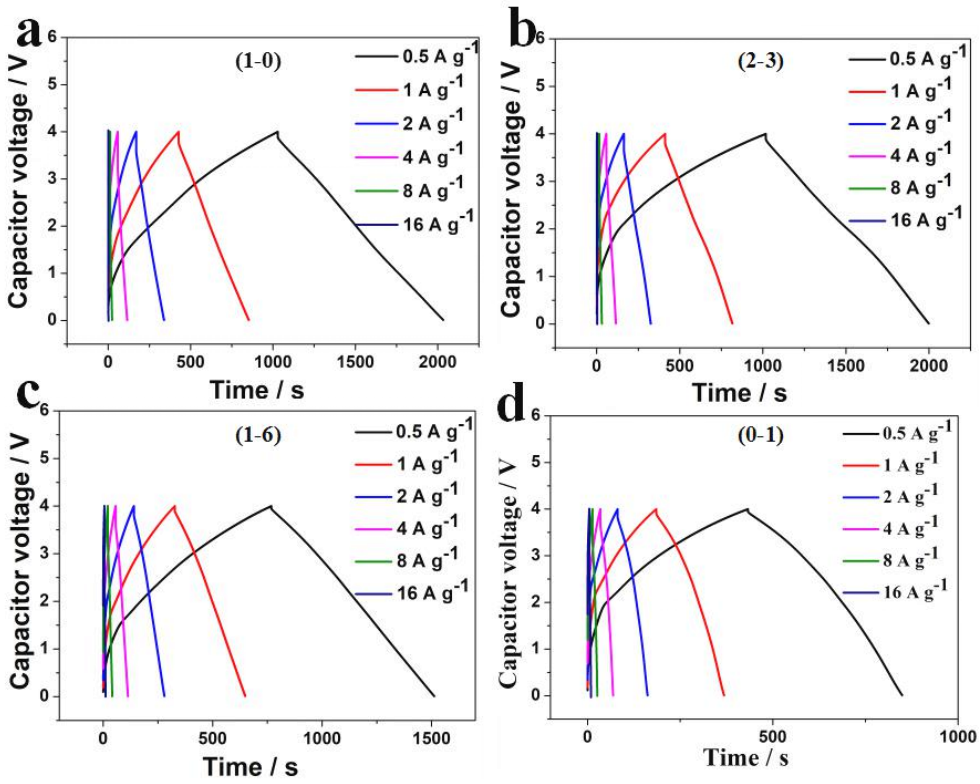

Fig. S26 Cycling stability and Coulombic efficiency of 4 V-KNCF//AC LICs (Ni:Co=1-0, 2-3, 1-6, 0-1) at 5 A g^{-1} with the anode precharged at 0.5 A g^{-1} and A electrolytes.

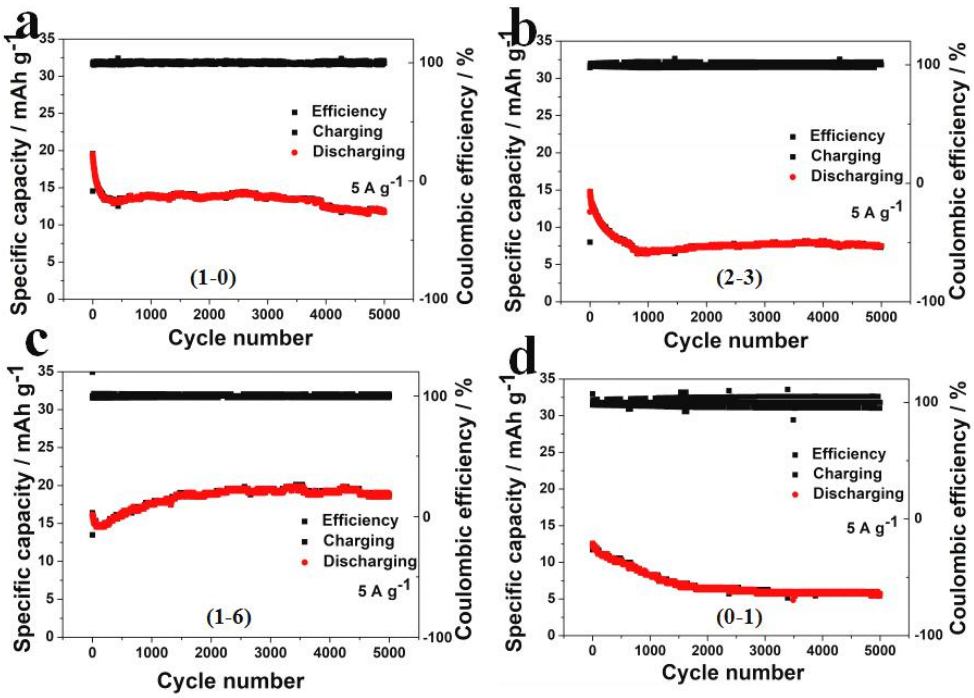

Fig. S27 LSV plots of AC electrode and the three-electrode potential monitor for KNCF(1-6)//AC LICs at 5 A g^{-1} with the anode precharged at 0.5 A g^{-1} and A electrolytes.

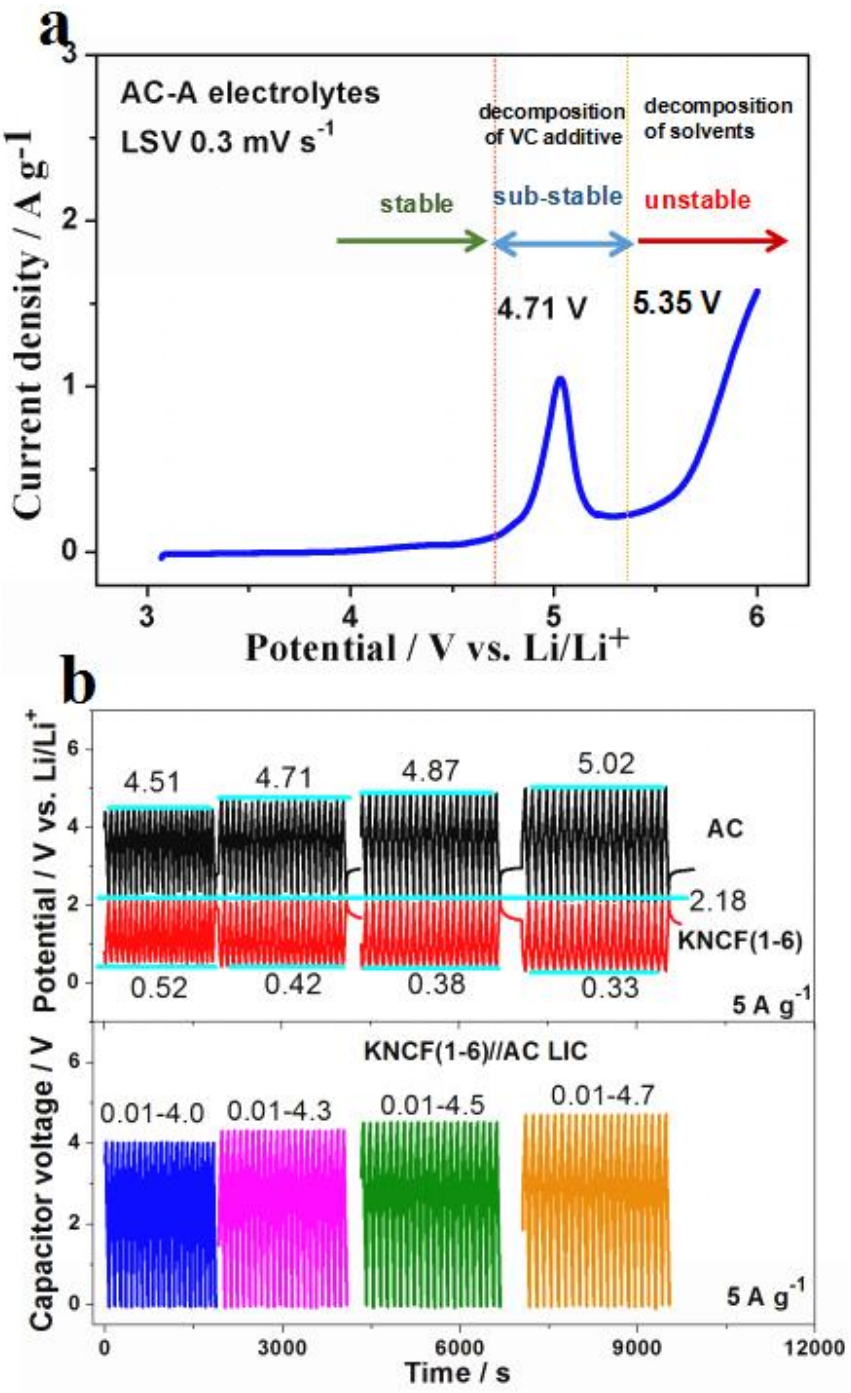

Fig. S28 CV plots at 10~160 mV s^{-1}, GCD curves at 0.5-16 A g^{-1}, Cycling stability and Coulombic efficiency at 5 A g^{-1} of 4.3 V-KNCF//AC LICs (Ni:Co=1-0, 1-6, 0-1) with the anode precharged at 0.5 A g^{-1} and A electrolytes.

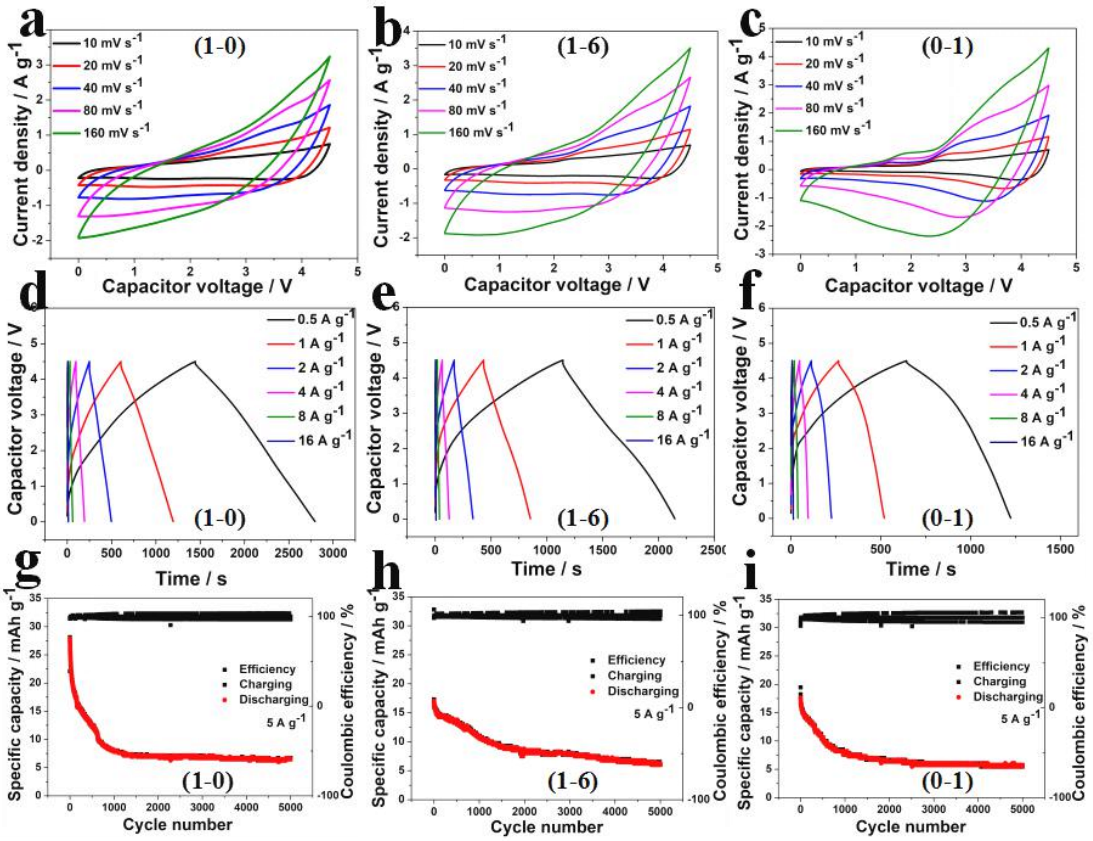

Fig. S29 CV plots at 10~160 mV s^{-1}, GCD curves at 0.5-16 A g^{-1}, Cycling stability and Coulombic efficiency at 5 A g^{-1} of 4.5 V-KNCF//AC LICs (Ni:Co=1-0, 1-6, 0-1) with the anode precharged at 0.5 A g^{-1} and A electrolytes.

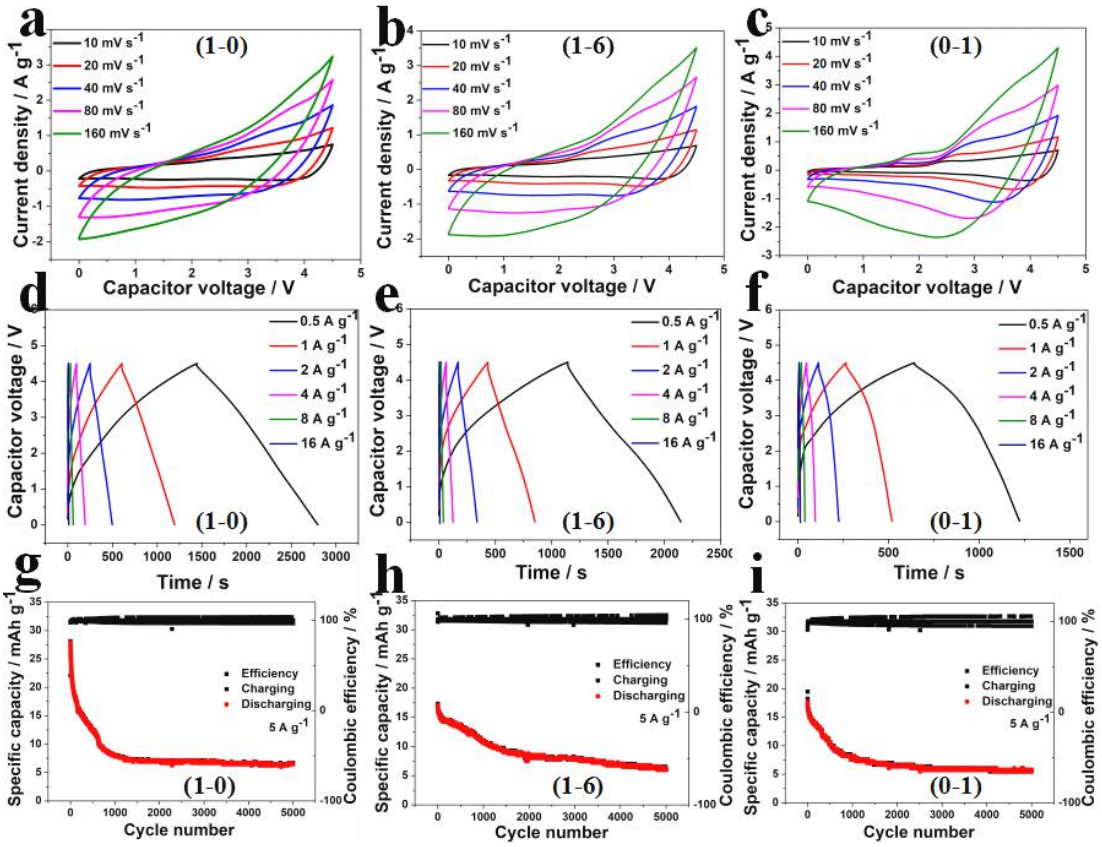

Fig. S30 CV plots at 10-160 mV s^{-1}, GCD curves at 0.5-16 A g^{-1}, Cycling stability and Coulombic efficiency at 5 A g^{-1} of 4.7 V-KNCF//AC LICs (Ni:Co=1-0, 1-6, 0-1) with the anode precharged at 0.5 A g^{-1} and A electrolytes.

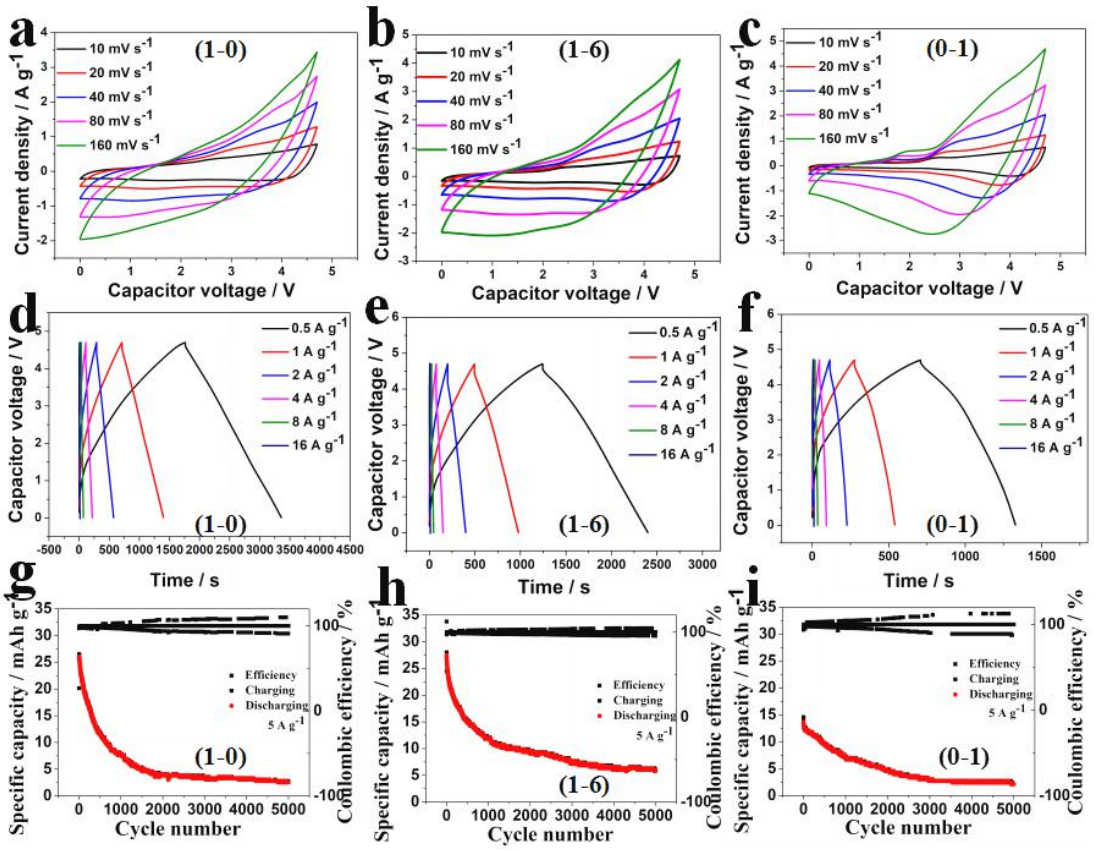

Fig. S31 CV plots at 10 mV s^{-1}, GCD curves at 1 A g^{-1}, Ragone plots and Cycling behavior of KNCF//AC LICs (1-0, 1-6, 0-1) under the voltages of 4.3 (1), 4.5 (2) and 4.7 (3) V with A electrolytes.

(1) 4.3 V

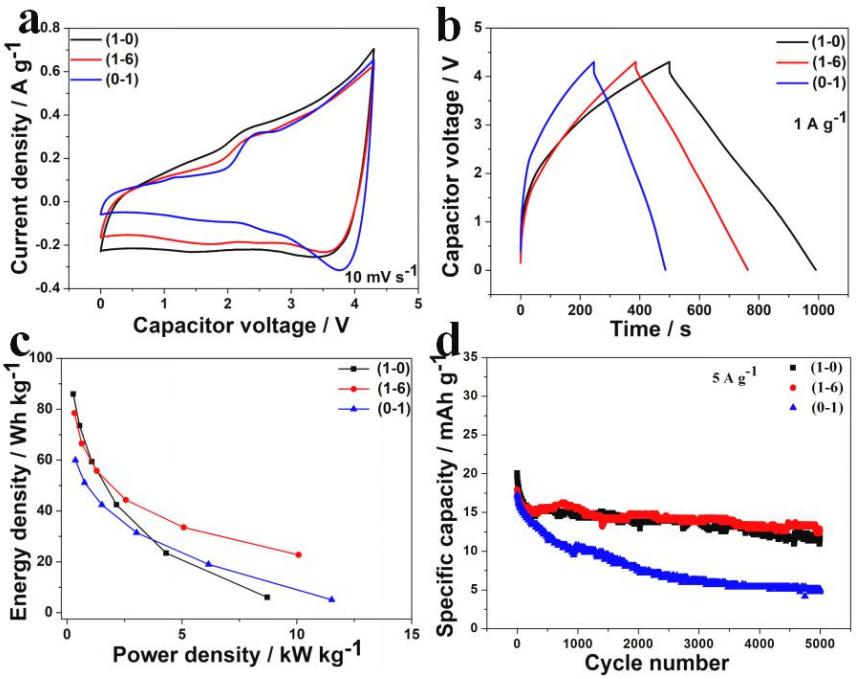

(2) 4.5 V

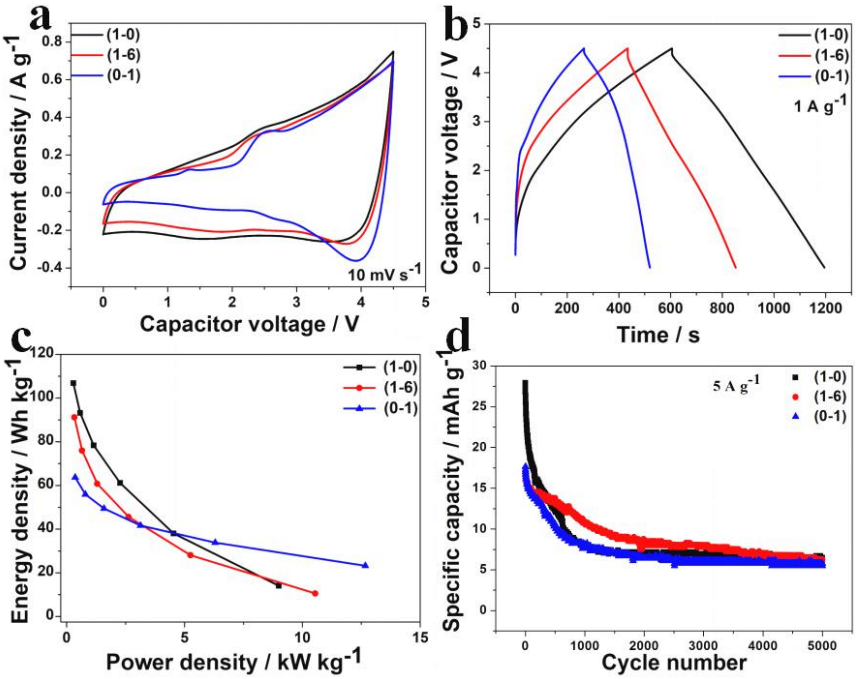

(3) 4.7V

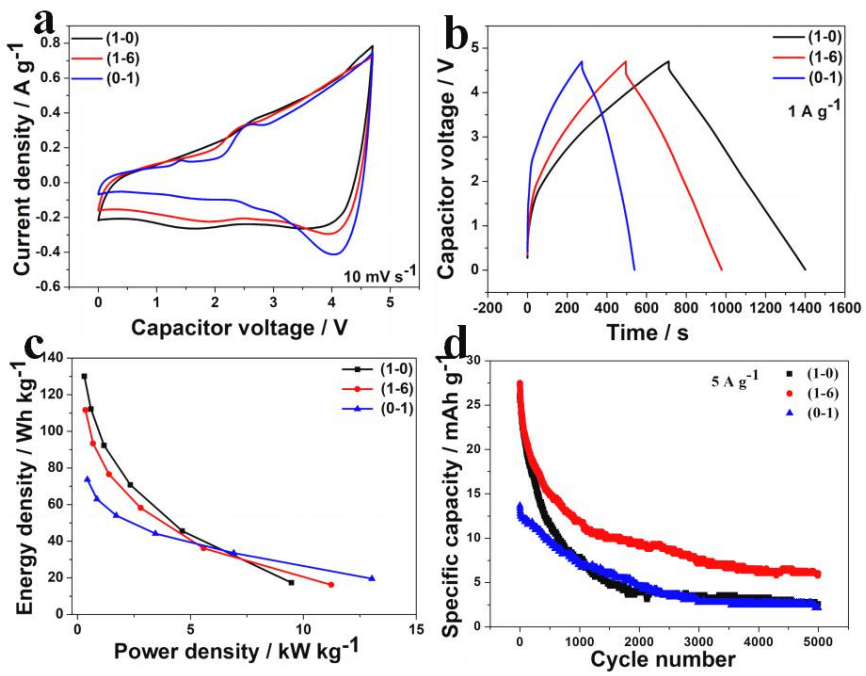

Fig. S32 GCD curves 0.1-3.2 A g^{-1} and CV plots at 0.3-160 mV s^{-1} of AC+LFP electrodes (1:1, 2:1, 4:1) with A electrolytes.

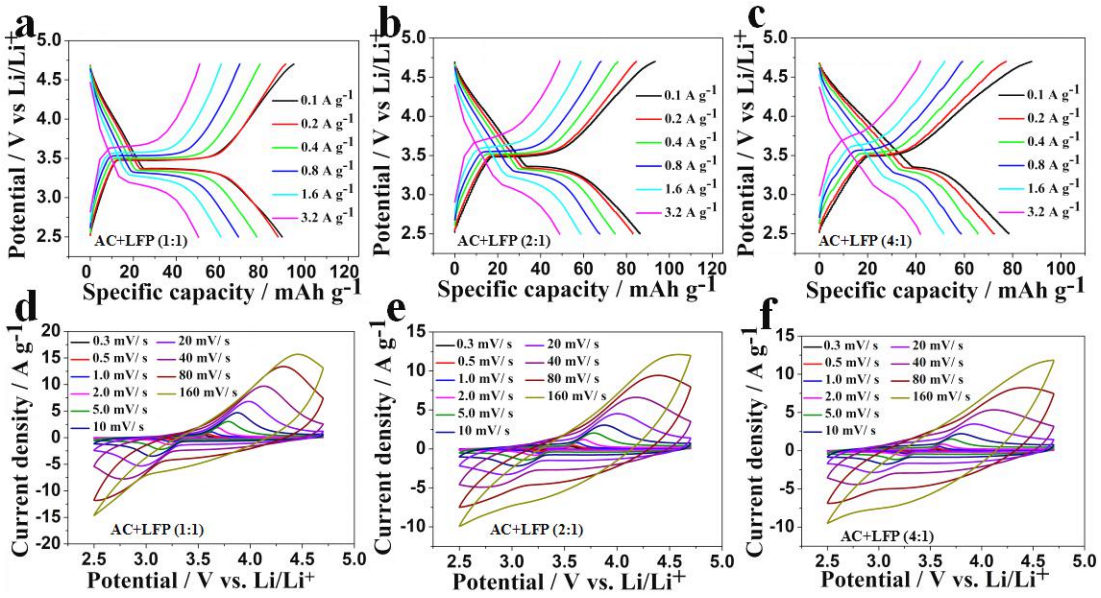

Fig. S33 CV plots at 10~160 mV s^{-1} of KNCF (1-6)//AC+LFP (1:1) LICs under different working voltages of 4~4.7 V with the anode precharged at 0.5 A g^{-1} and A electrolytes.

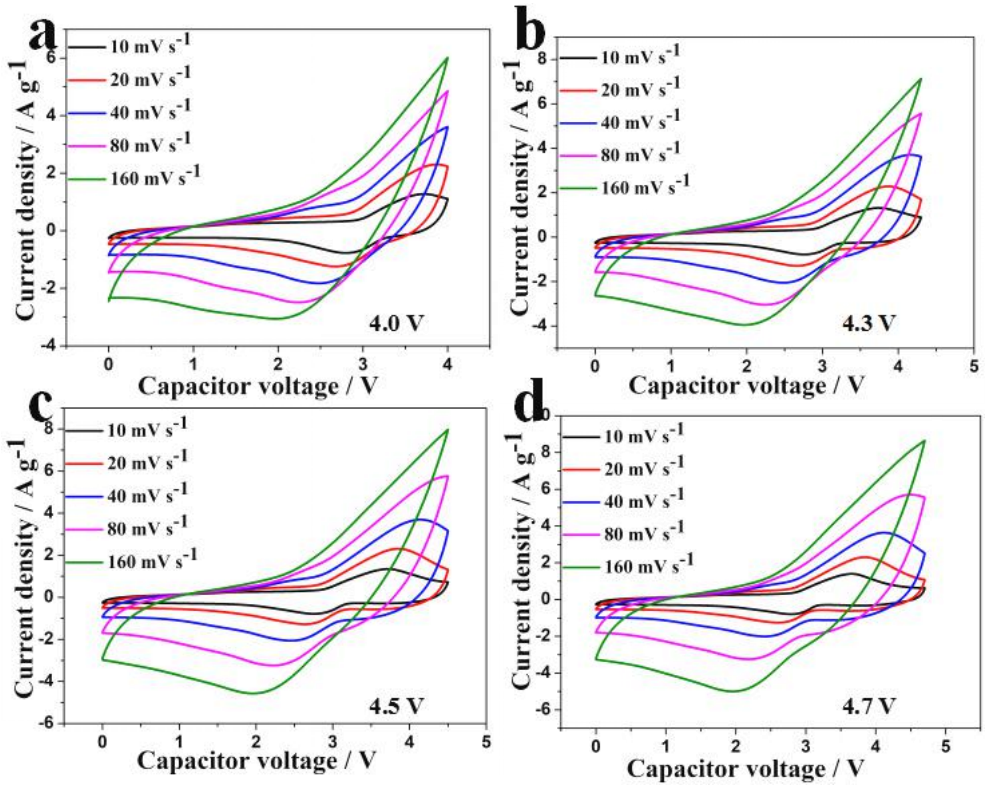

Fig. S34 GCD curves 0.5~16 A g^{-1} of KNCF (1-6)//AC+LFP (1:1) LICs under different working voltages of 4~4.7 V with the anode precharged at 0.5 A g^{-1} and A electrolytes.

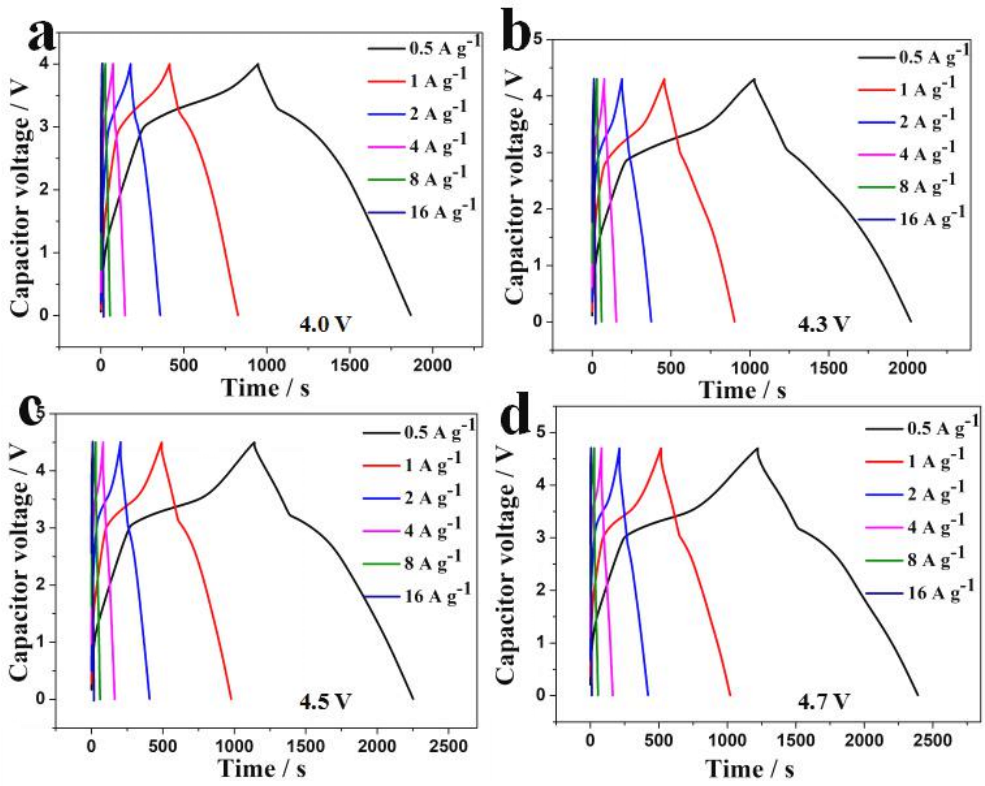

Fig. S35 CV plots at 10 mV s^{-1}, GCD curves at 1 A g^{-1}, Ragone plots and cycling behavior of KNCF (1-6)//AC+LFP (1:1) LICs under different working voltages of 4~4.7 V with the anode precharged at 0.5 A g^{-1} and A electrolytes.

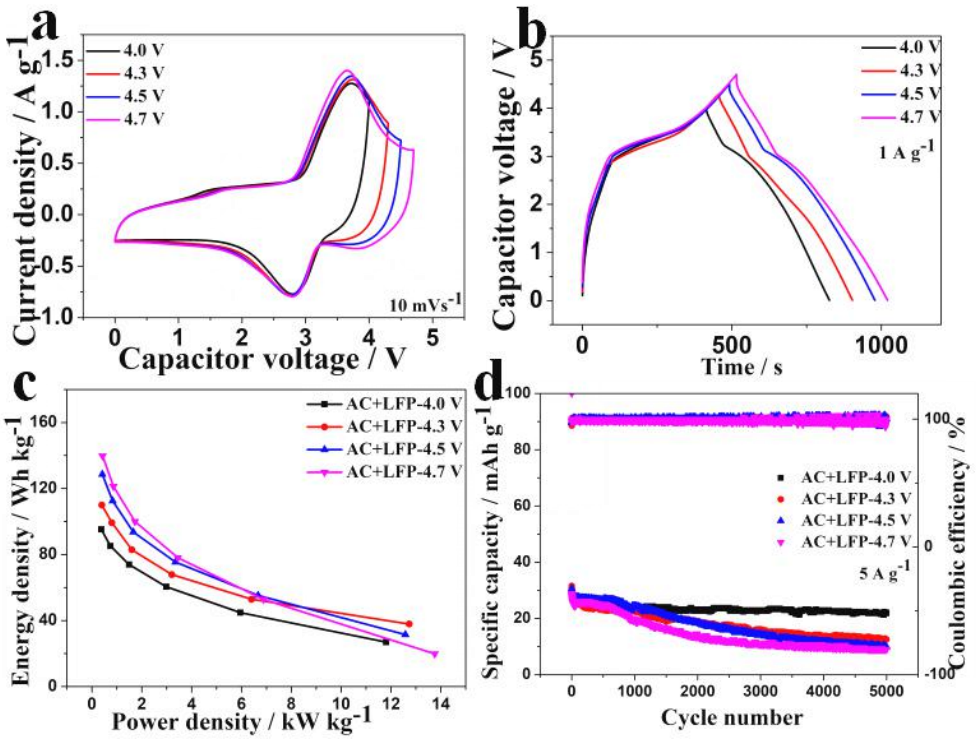

Fig. S36 Performance of LFP electrode with A electrolytes: CV plots at 0.3~20 mV s^{-1}(a), GCD curves at 0.1 A g^{-1} for the first five cycles (b) and different current densities (c), rate performance (d, e) and cycling behavior (f).

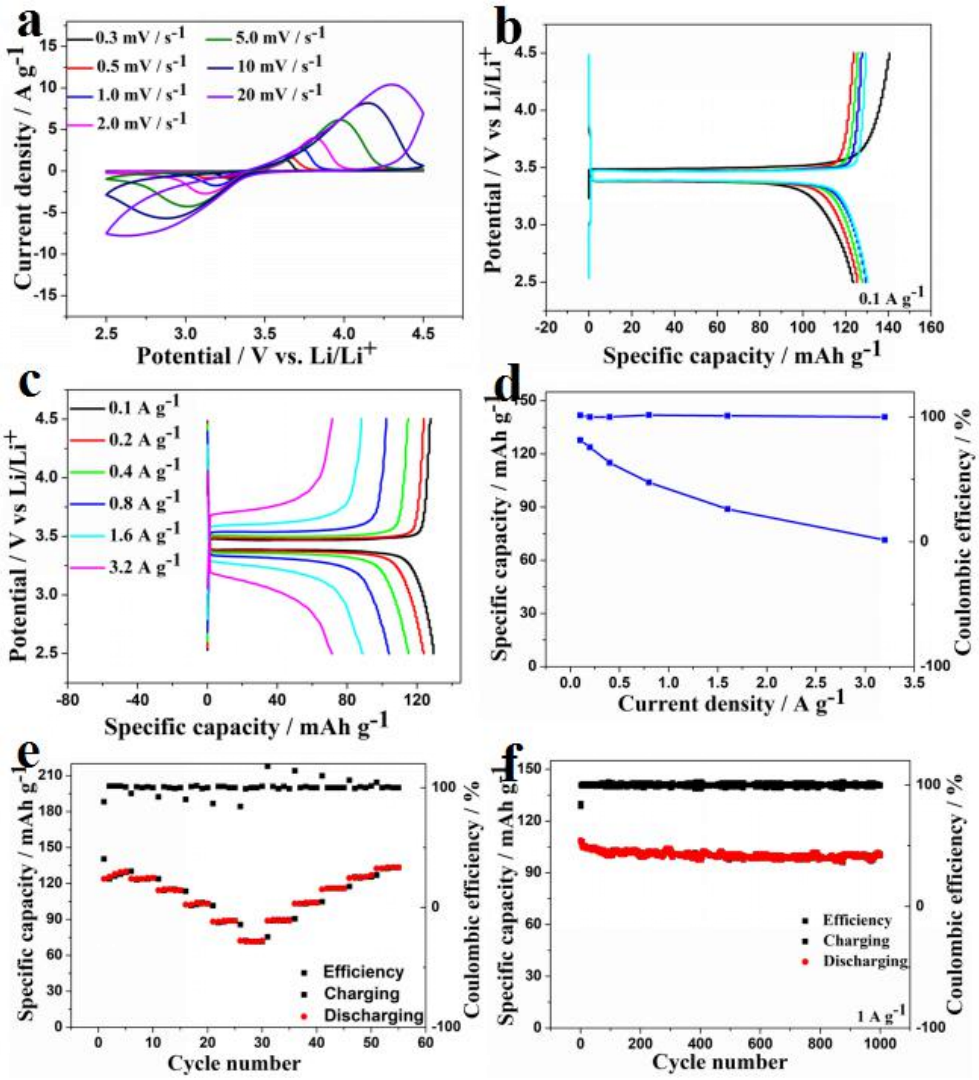

Fig. S37 Performance of KNCF(1-6)//LFP LIB with the anode precharged at 0.5 A g^{-1} and A electrolytes: CV windows at 10 mV s^{-1}(a), CV plots at 10~160 mV s^{-1} (b), GCD curves at 0.5-16 A g^{-1} (c), Ragone behavior (d) and cycling behavior (e).

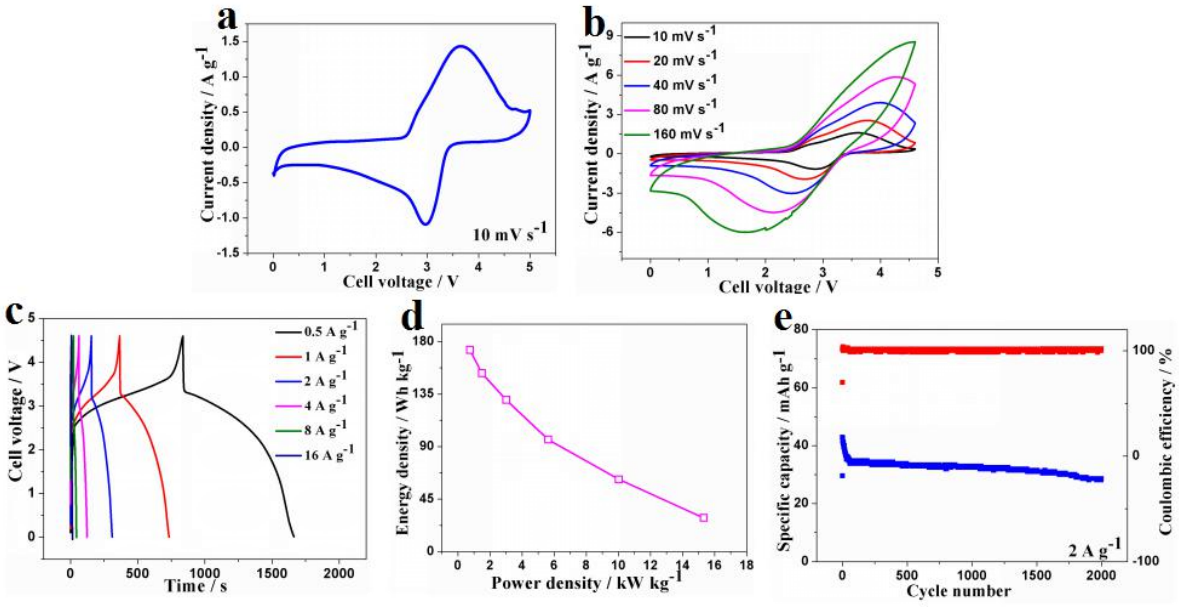

Fig. S38 CV plots at 10~160 mV s^{-1} of KNCF (1-6)//AC LICs under different working voltages of 4~4.7 V with both the anode and cathode precharged at 0.5 A g^{-1} and A electrolytes.

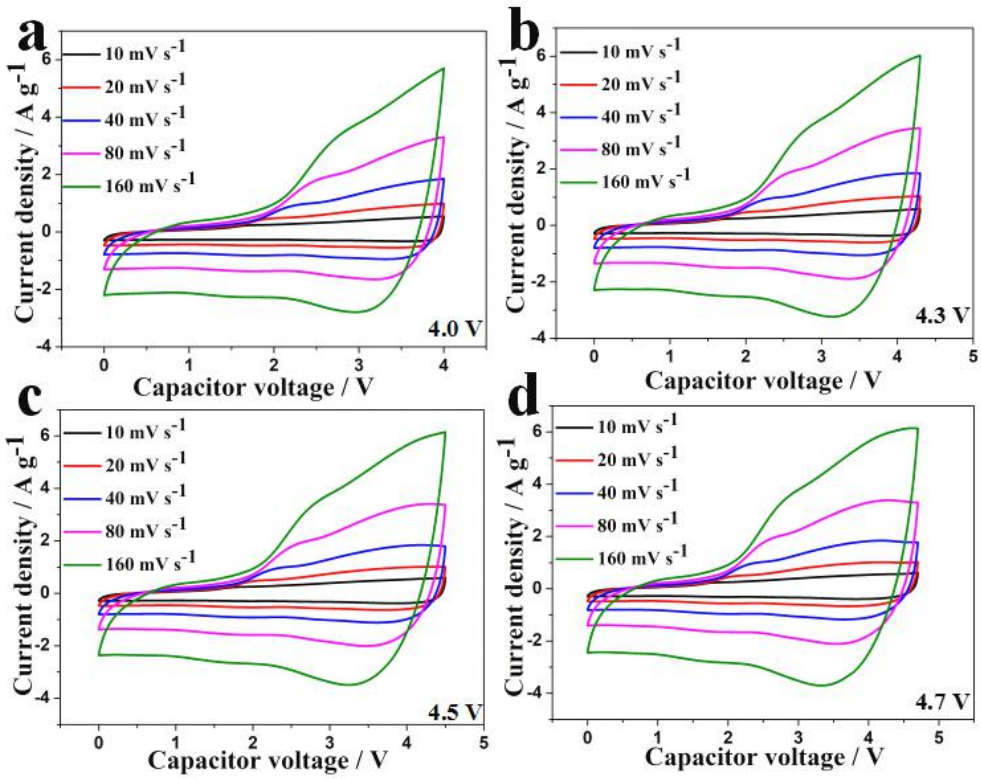

Fig. S39 GCD curves 0.5~16 A g^{-1} of KNCF (1-6)//AC LICs under different working voltages of 4~4.7 V with both the anode and cathode precharged at 0.5 A g^{-1} and A electrolytes.

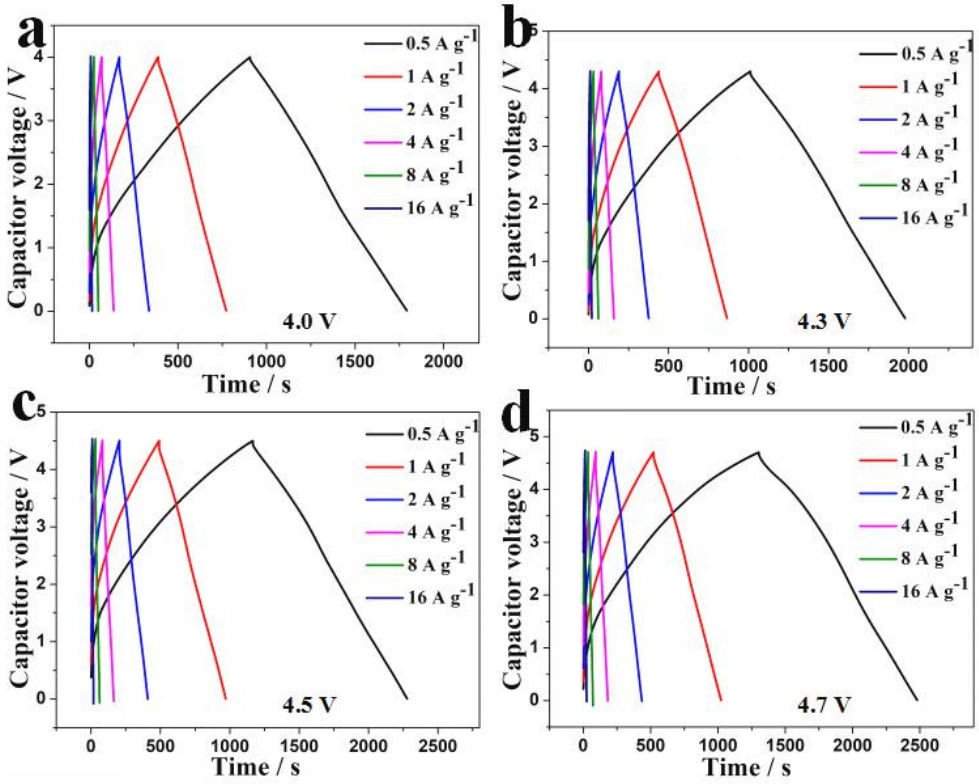

Fig. S40 CV plots at 10 mV s^{-1}, GCD curves at 1 A g^{-1}, Ragone plots and cycling behavior of KNCF (1-6)//AC LICs under different working voltages of 4~4.7 V with the anode precharged at 0.5 A g^{-1} and A electrolytes.

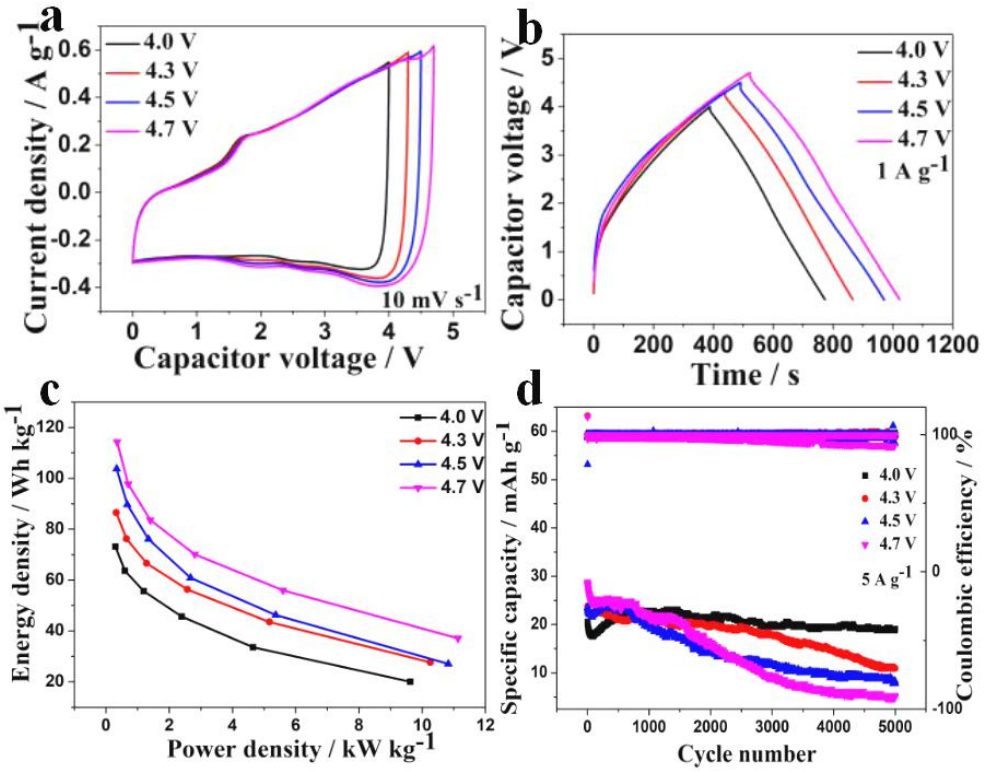

Fig. S41 CV plots at 0.3 mV $s^{-1}$for the first three cycles of graphite electrodes (918, SAG, KS6) with A and B (for 918) or B (for SAG, KS6) electrolytes.

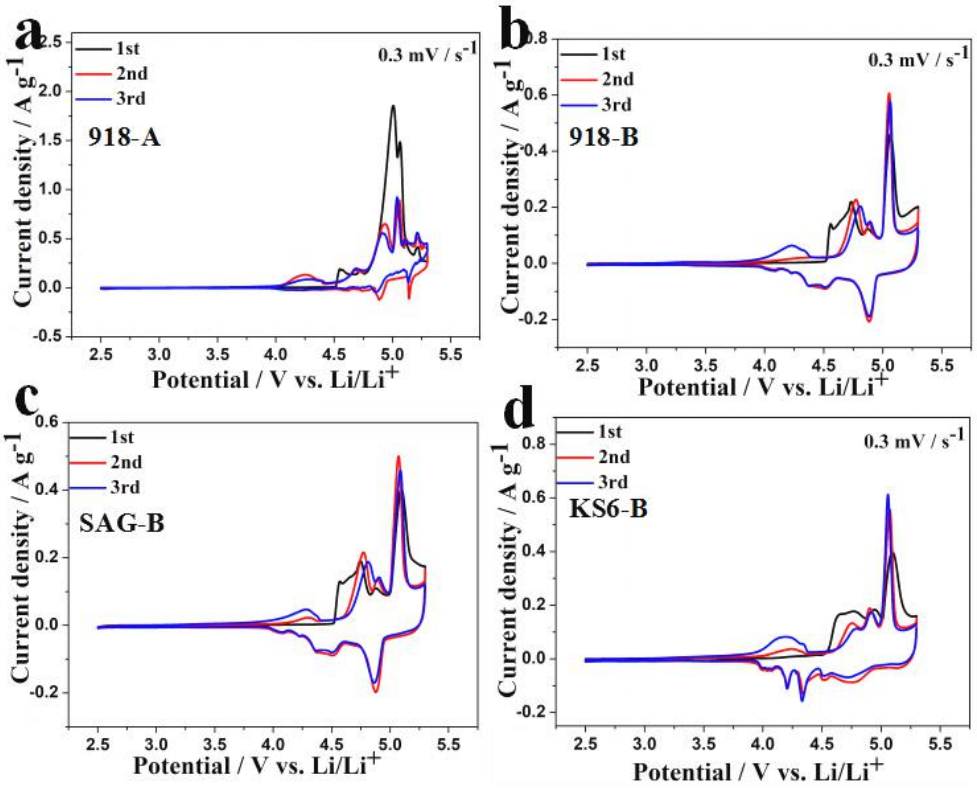

Fig. S42 GCD curves at 0.1 A g^{-1} for the first five cycles of graphite electrodes (918, SAG, KS6) with A and B (for 918) or B (for SAG, KS6) electrolytes.

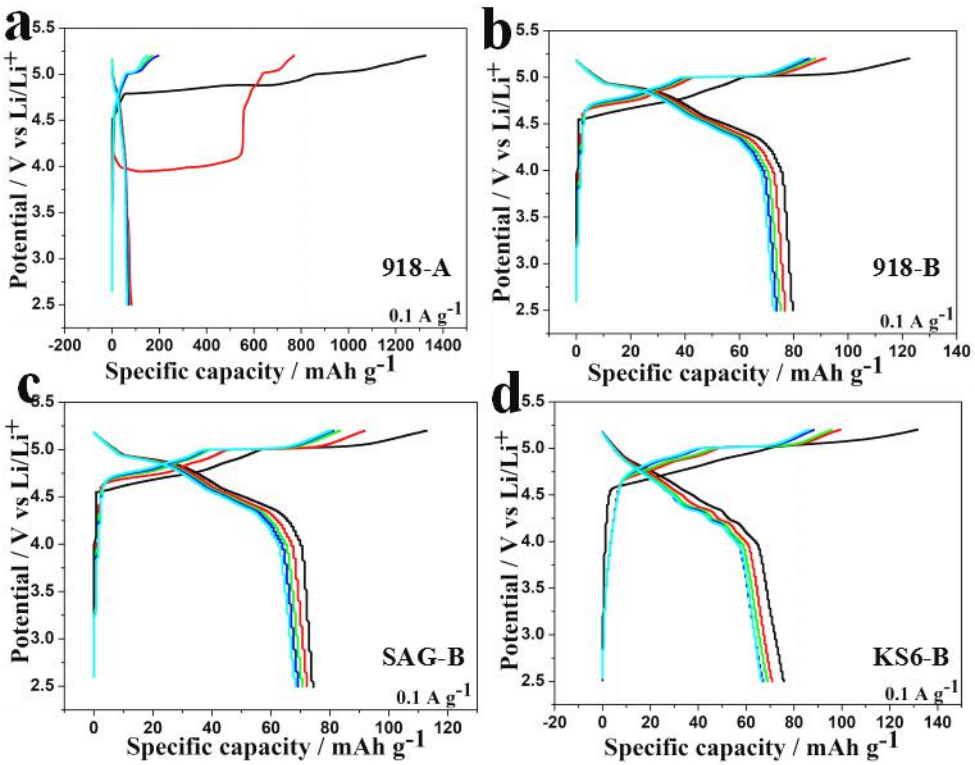

Fig. S43 GCD curves at 0.1 A g^{-1} for the first five cycles of 918, 918+AC (1:1), 918+LFP (1:1) and 918+AC+LFP (1:1:1) electrodes with B electrolytes.

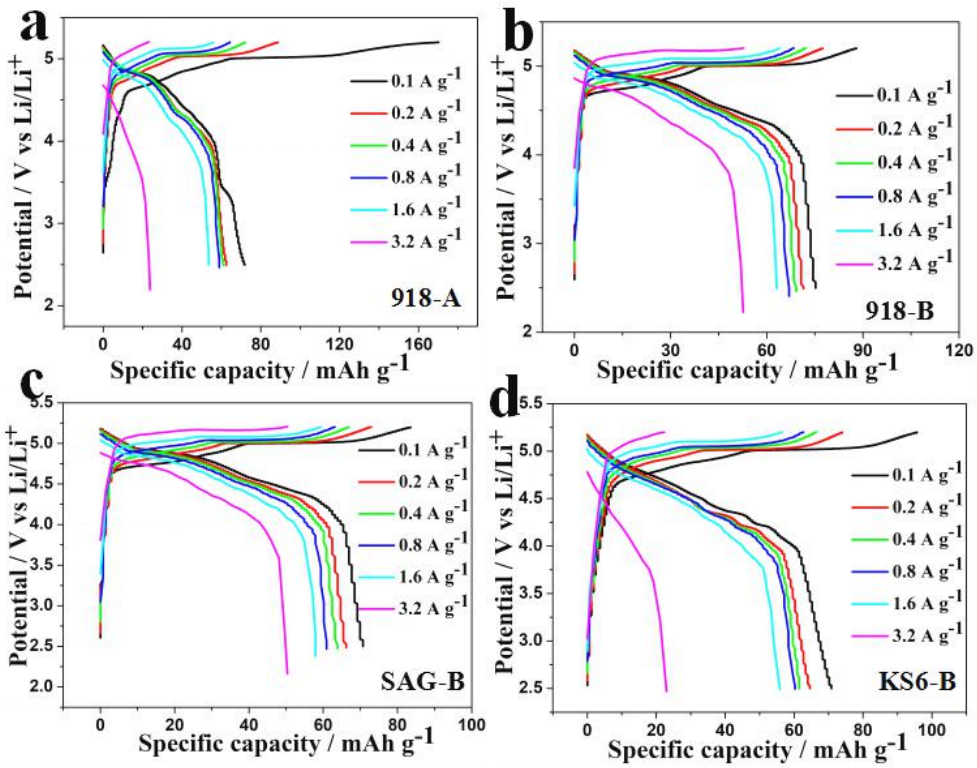

Fig. S44 CV plots at 0.3 mV $s^{-1}$for the first three cycles of 918, 918+AC (1:1), 918+LFP (1:1) and 918+AC+LFP (1:1:1) electrodes with B electrolytes.

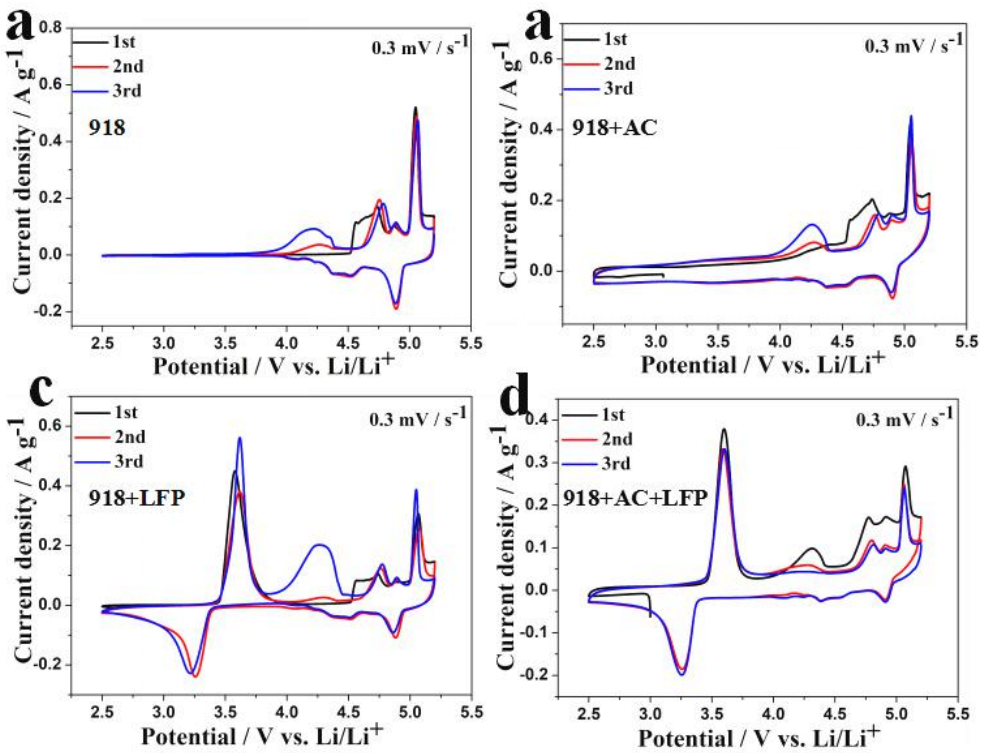

Fig. S45 GCD curves at 0.1 A g^{-1} for the first five cycles of 918, 918+AC (1:1), 918+LFP (1:1) and 918+AC+LFP (1:1:1) electrodes with B electrolytes.

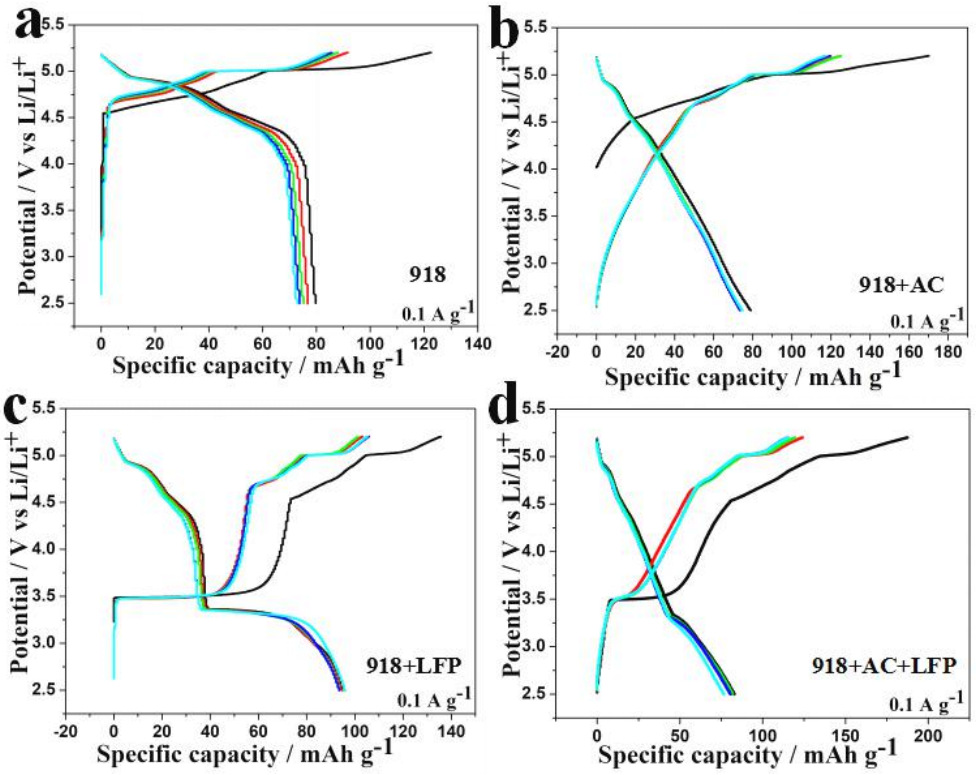

Fig. S46 GCD curves at 0.1~3.2 A g^{-1} of 918, 918+AC (1:1), 918+LFP (1:1) and 918+AC+LFP (1:1:1) electrodes with B electrolytes.

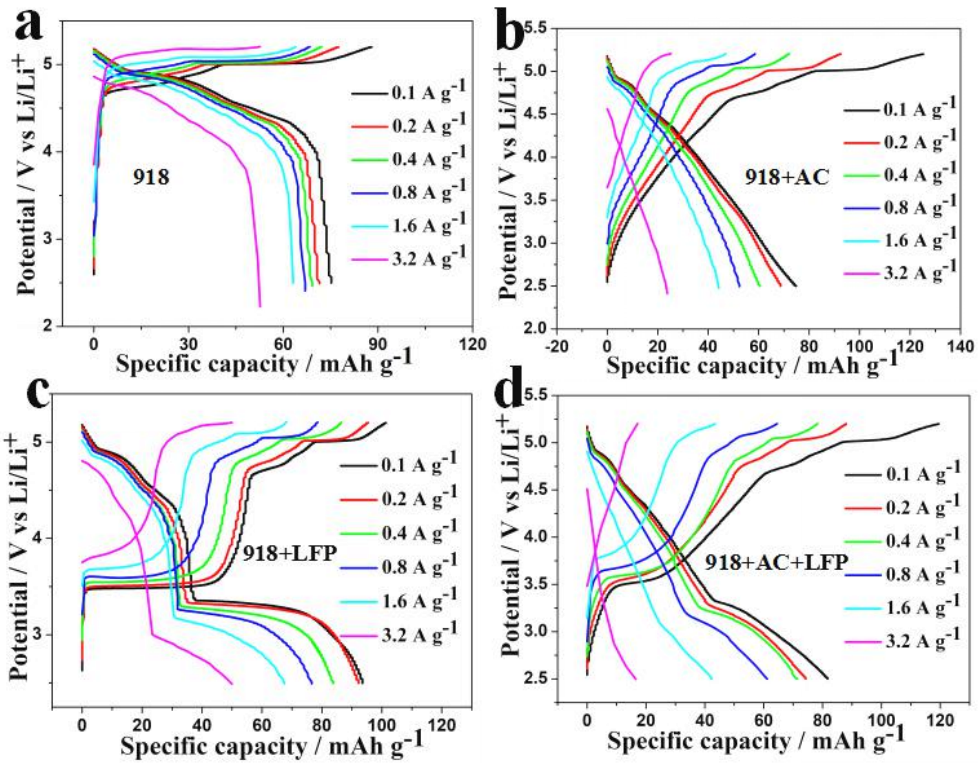

Fig. S47 LSV plots of 918, 918+AC (1:1), 918+LFP (1:1), 918+AC+LFP (1:1:1), KS6 and SAG electrodes at 0.3 mV s^{-1} with B electrolytes.

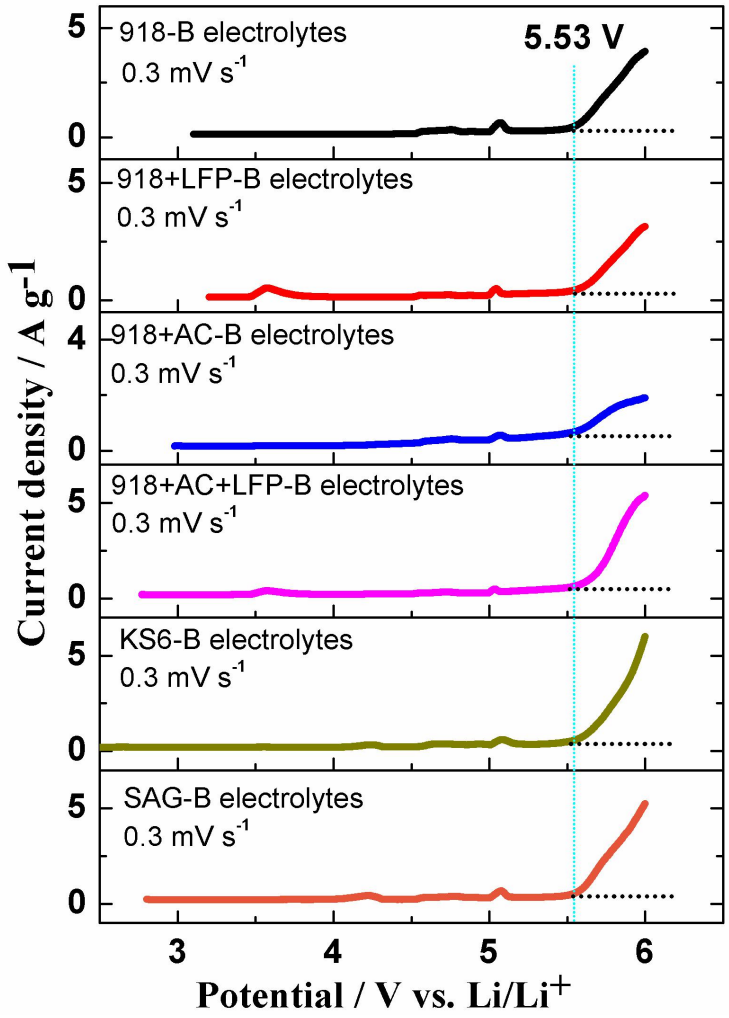

Fig. S48 CV plots at 0.3 mV s^{-1}, GCD curves at 0.1~3.2 A g^{-1}, rate performance and cycling behavior of KNCF (1-6) electrode with B electrolytes.

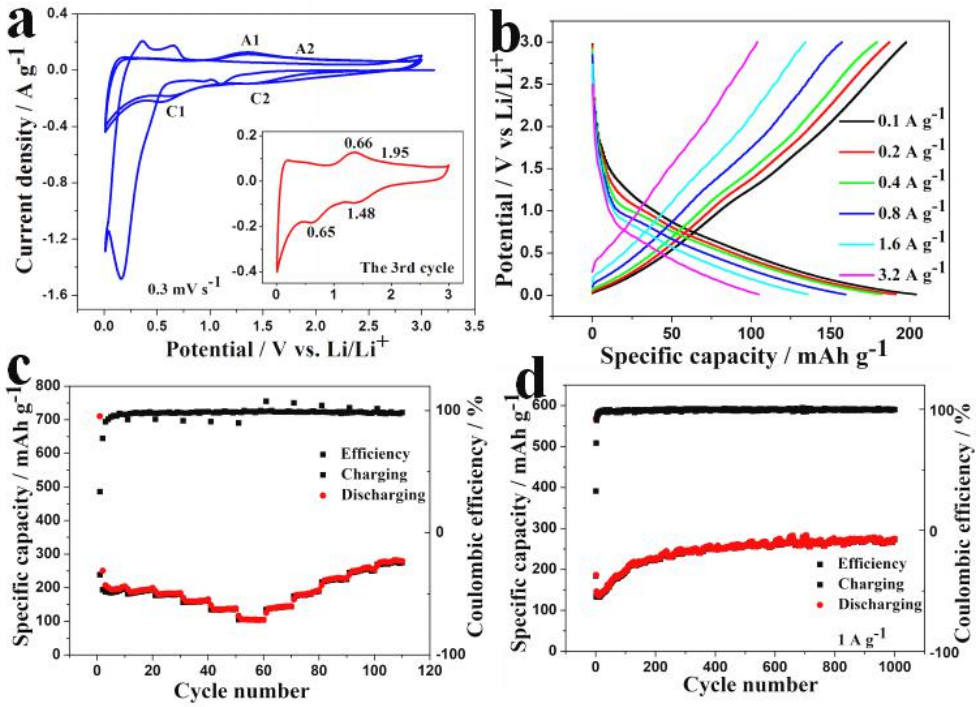

Fig. S49 CV plots at 10~160 mV s^{-1} of KNCF (1-6)//(918, 918+AC, 918+LFP, 918+AC+LFP) DIBs under the working voltages of 0.5-5.2 V with the anode precharged at 0.5 A g^{-1} and B electrolytes.

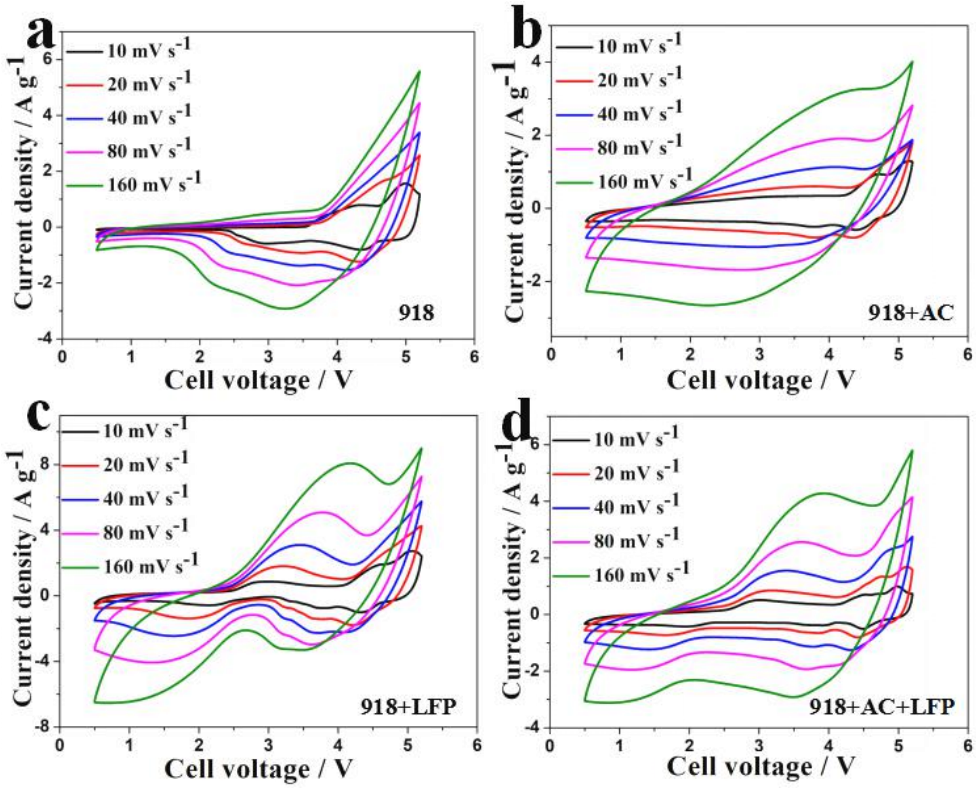

Fig. S50 GCD curves at 0.5~8 A g^{-1} of KNCF (1-6)//(918, 918+AC, 918+LFP, 918+AC+LFP) DIBs under the working voltages of 0.5-5.2 V with the anode precharged at 0.5 A g^{-1} and B electrolytes.

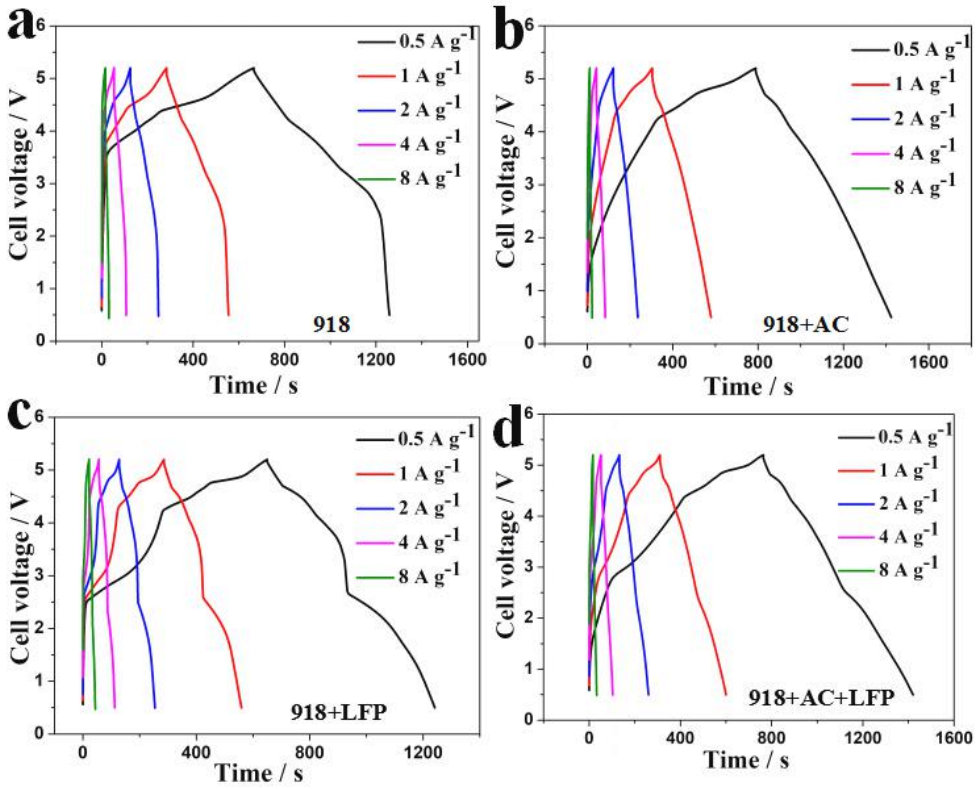

Fig. S51 CV plots at 10~160 mV s^{-1} of KNCF (1-6)//(918, 918+AC, 918+LFP, 918+AC+LFP) DIBs under the working voltages of 0.5-5.5 V with the anode precharged at 0.5 A g^{-1} and B electrolytes.

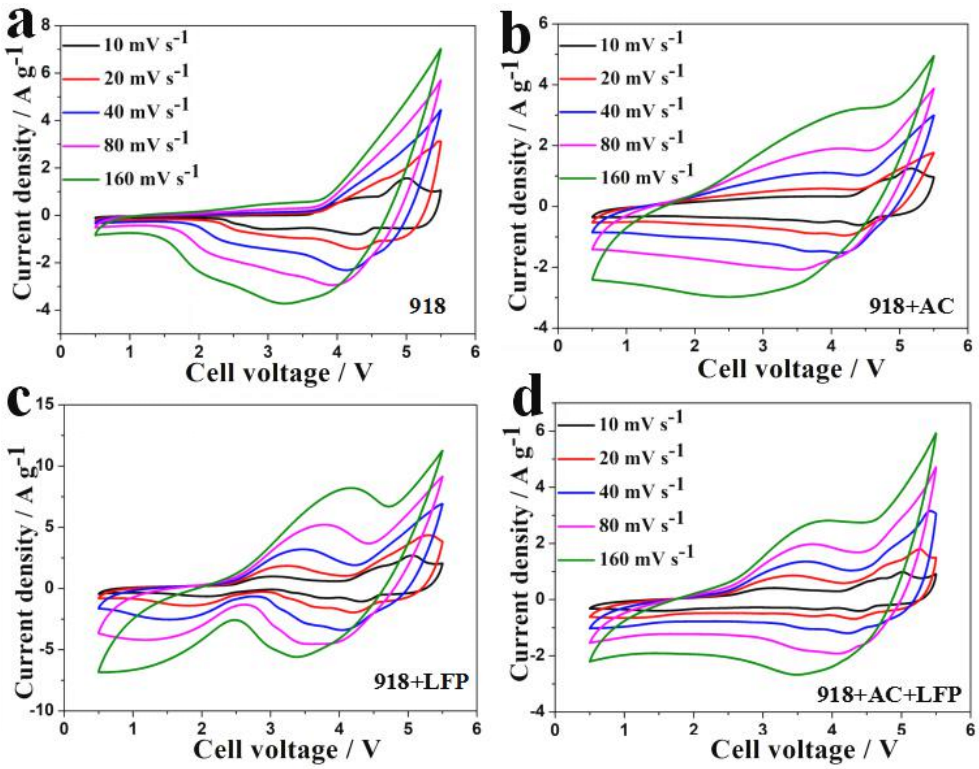

Fig. S52 GCD curves at 0.5~8 A g^{-1} of KNCF (1-6)//(918, 918+AC, 918+LFP, 918+AC+LFP) DIBs under the working voltages of 0.5-5.5 V with the anode precharged at 0.5 A g^{-1} and B electrolytes.

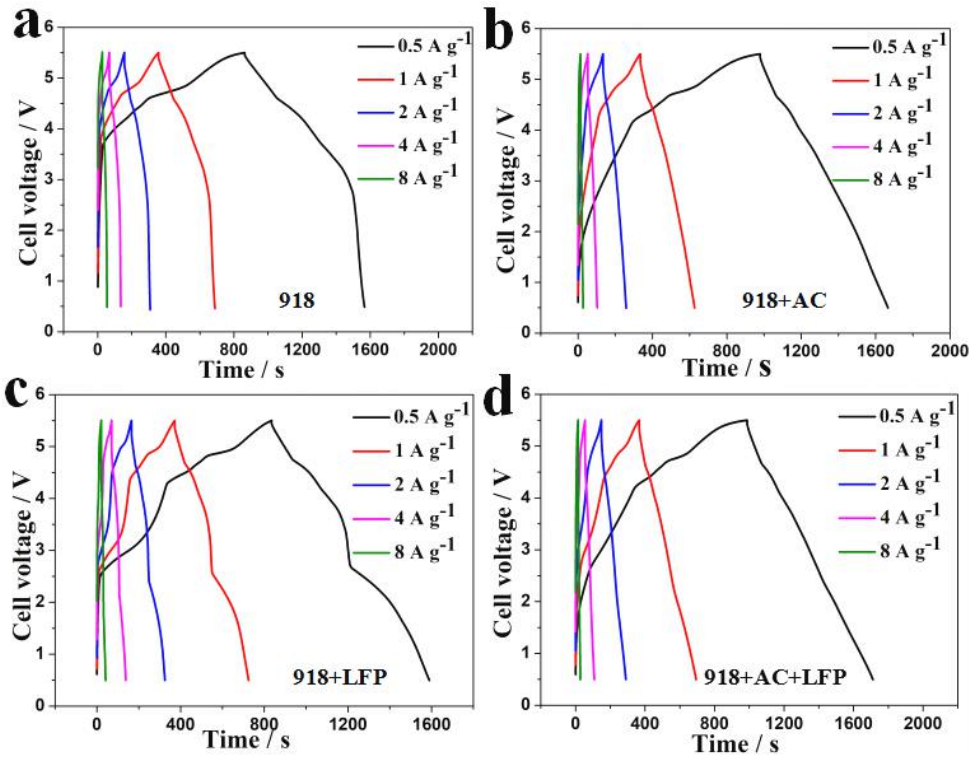

Fig. S53 Performance of KNCF(1-6)//SAG DIB under 1-5.2 V and 1-5.5 V with the anode precharged at 0.5 A g^{-1} and B electrolytes: CV windows at 10 mV s^{-1}(a), CV plots at 10~160 mV s^{-1} (b, c), GCD curves at 0.5-8 A g^{-1} (e, f), Ragone behavior (d, g) and cycling behavior (h, i).

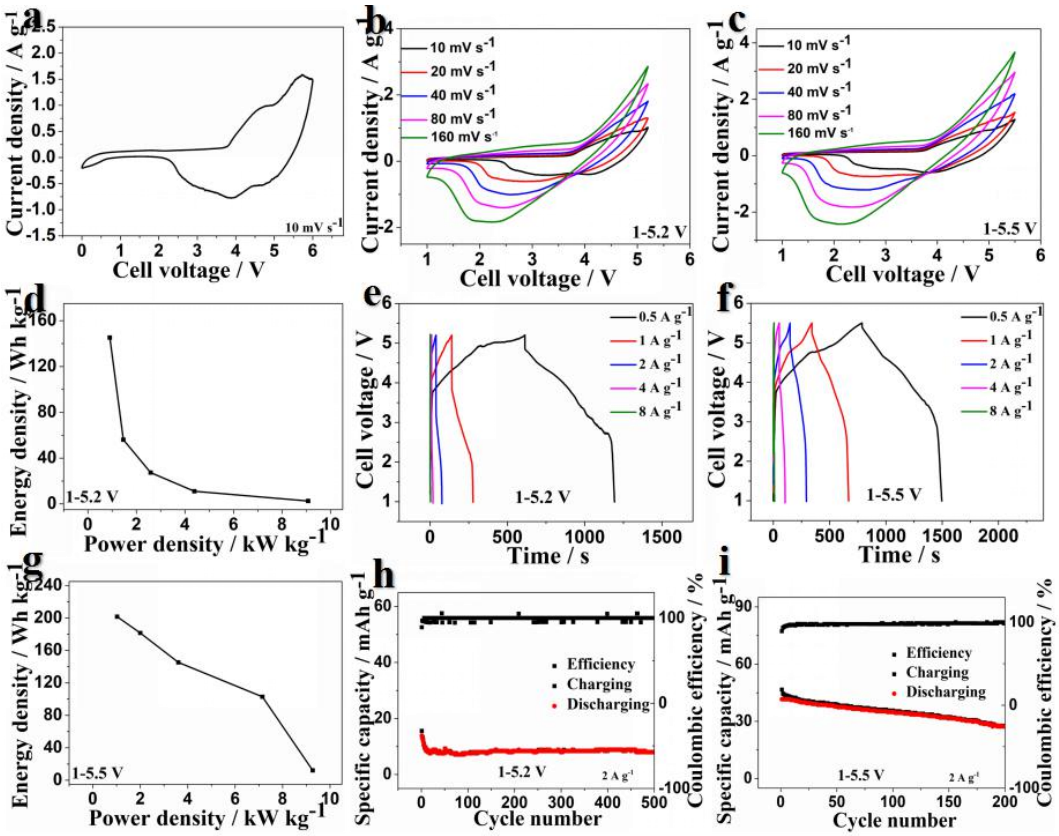

Fig. S54 Performance of KNCF(1-6)//KS6 DIB under 1-5.2 V and 1-5.5 V with the anode precharged at 0.5 A g^{-1} and B electrolytes: CV windows at 10 mV s^{-1} (a), CV plots at 10~160 mV s^{-1} (b, c), GCD curves at 0.5-8 A g^{-1} (e, f), Ragone behavior (d, g) and cycling behavior (h, i).

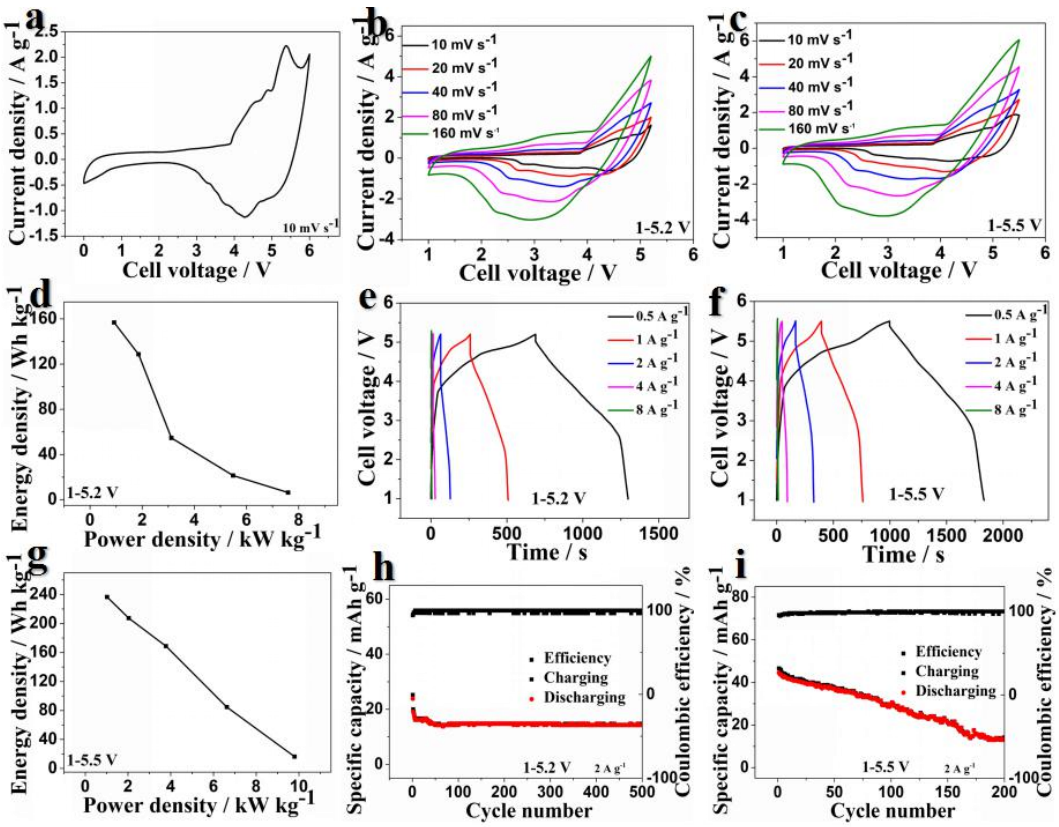

Fig. S55 Performance of KNCF (1-6)//AC LIC with the anode precharged and A electrolytes under low temperature (-20 ℃): (a) CV windows at 30 mV s^{-1}, (b) CV plots at 10-160 mV s^{-1}, (c) GCD curves at 0.5-8 A g^{-1}, (d) rate performance, (e) Ragone behavior and (f) cycling behavior.

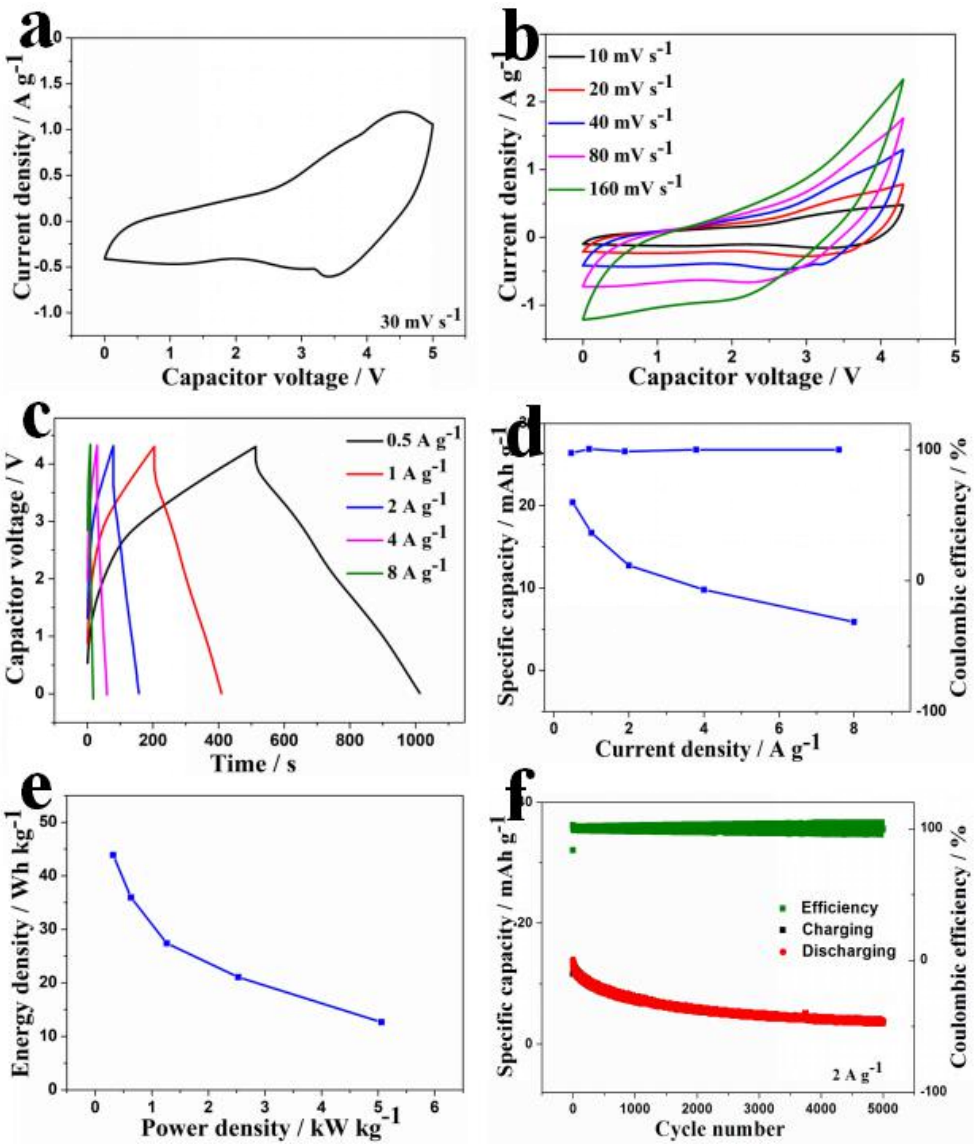

Fig. S56 Performance of KNCF (1-6)//AC+LFP (1:1) LIC with the anode precharged and A electrolytes under low temperature (-20 ℃): (a) CV windows at 30 mV s^{-1}, (b) CV plots at 10-160 mV s^{-1}, (c) GCD curves at 0.5-8 A g^{-1}, (d) rate performance, (e) Ragone behavior and (f) cycling behavior.

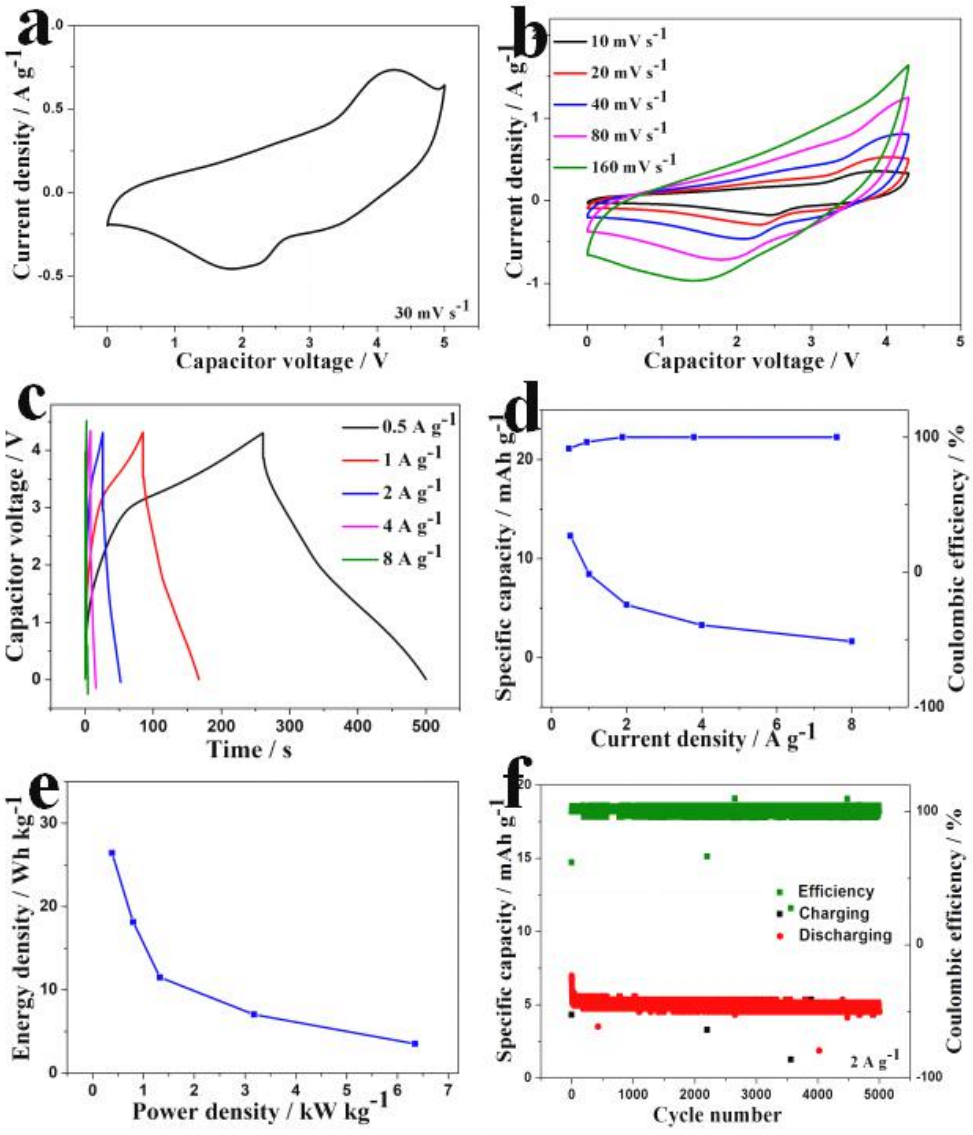

Fig. S57 Performance of KNCF (1-6)//AC LIC with both the anode and cathode precharged and A electrolytes under low temperature (-20 ℃): (a) CV windows at 30 mV s^{-1}, (b) CV plots at 10-160 mV s^{-1}, (c) GCD curves at 0.5-8 A g^{-1}, (d) rate performance, (e) Ragone behavior and (f) cycling behavior.

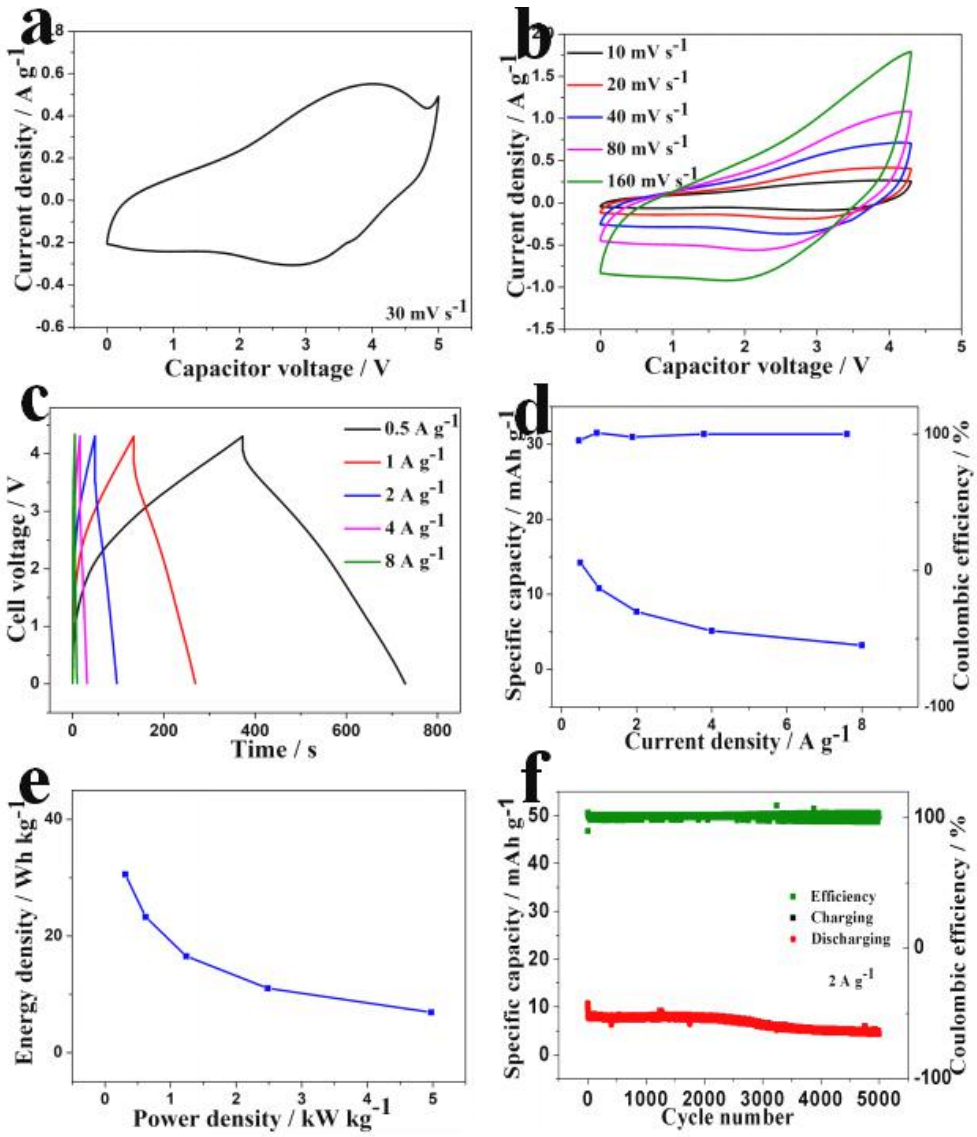

Fig. S58 Performance of KNCF (1-6)//918 DIB with the anode precharged and B electrolytes under low temperature (-20 ℃): (a) CV windows at 10 mV s^{-1}, (b) CV plots at 10-160 mV s^{-1}, (c) GCD curves at 0.5-8 A g^{-1}, (d) rate performance, (e) Ragone behavior and (f) cycling behavior.

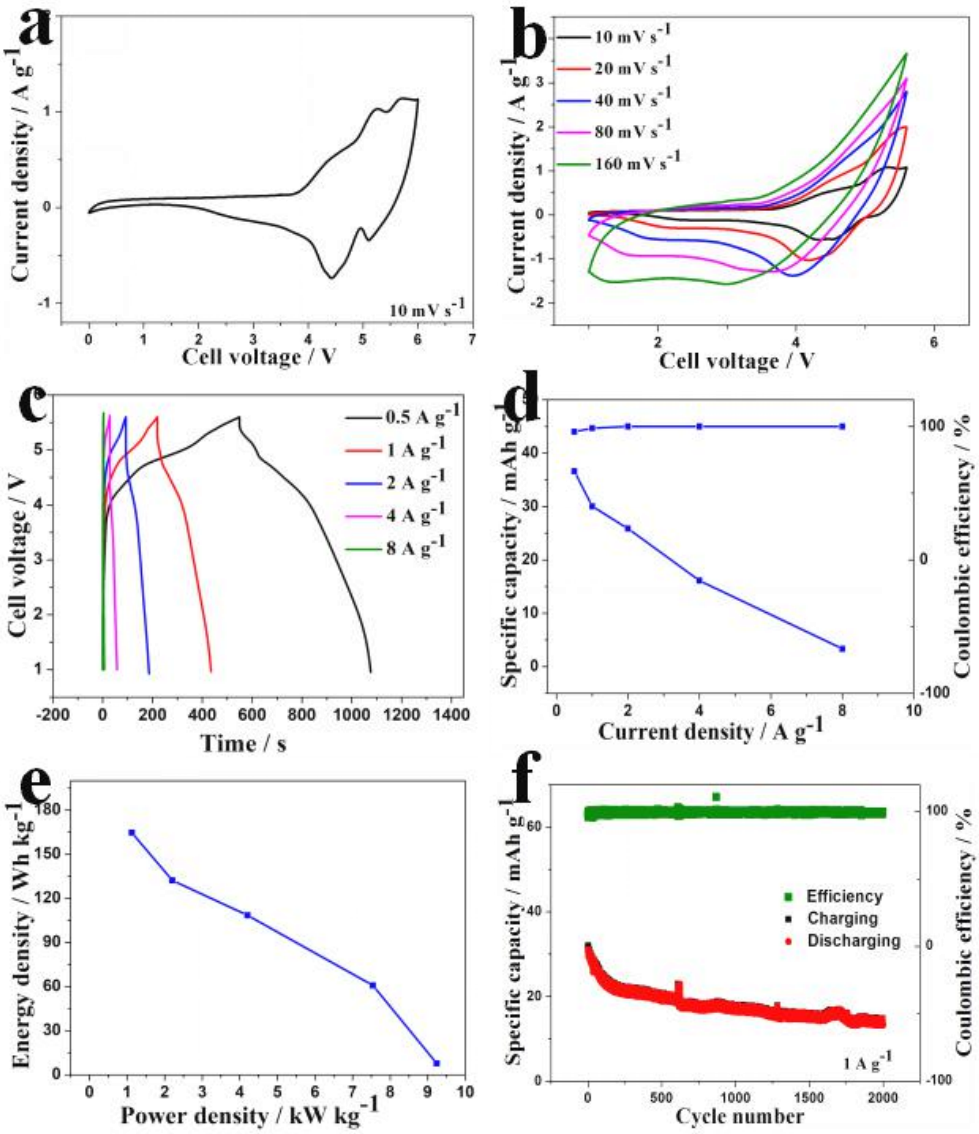

Fig. S59 Performance of KNCF (1-6)//AC LIC with the anode precharged and A electrolytes under high temperature (40 ℃): (a) CV windows at 30 mV s^{-1}, (b) CV plots at 10-160 mV s^{-1}, (c) GCD curves at 0.5-8 A g^{-1}, (d) rate performance, (e) Ragone behavior and (f) cycling behavior.

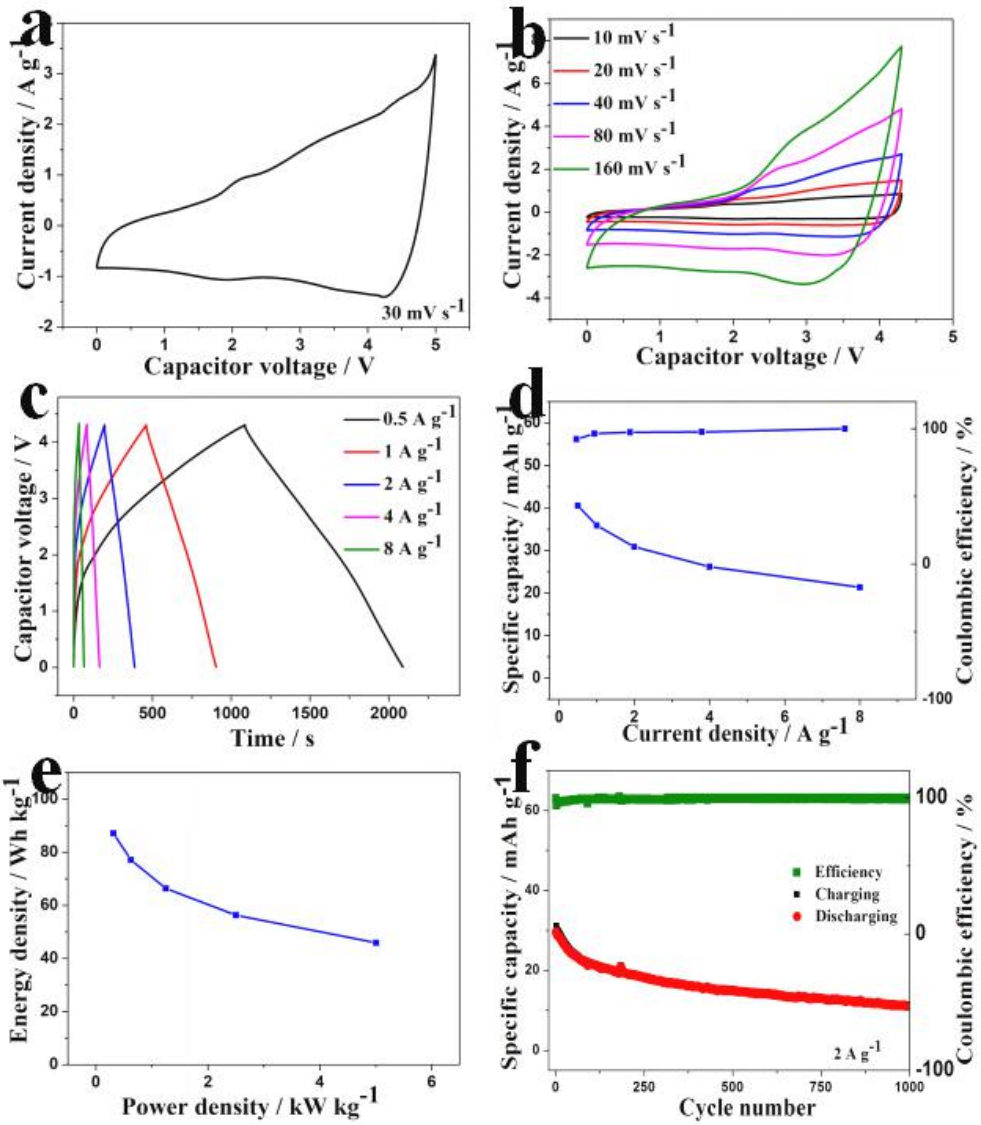

Fig. S60 Performance of KNCF (1-6)//AC+LFP (1:1) LIC with the anode precharged and A electrolytes under high temperature (40 ℃): (a) CV windows at 30 mV s^{-1}, (b) CV plots at 10-160 mV s^{-1}, (c) GCD curves at 0.5-8 A g^{-1}, (d) rate performance, (e) Ragone behavior and (f) cycling behavior.

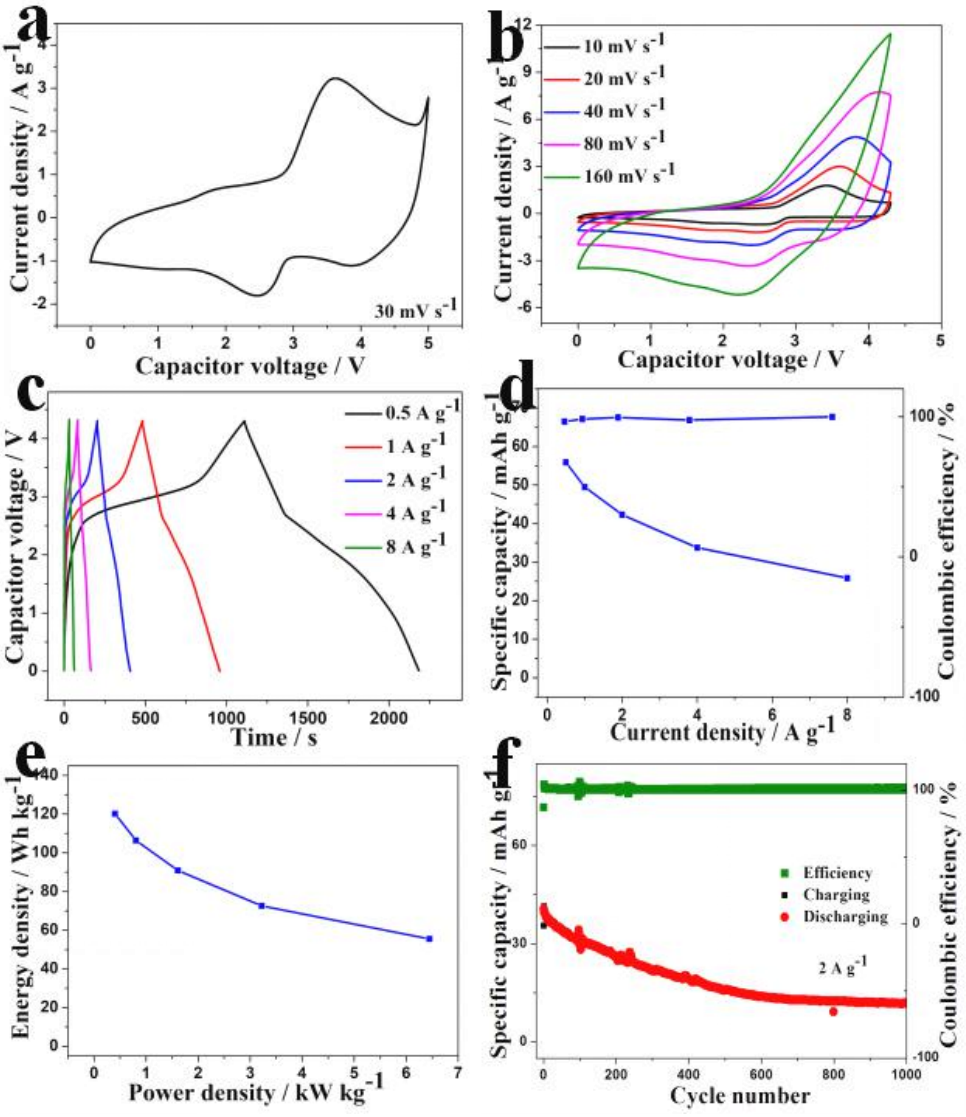

Fig. S61 Performance of KNCF (1-6)//AC LIC with both the anode and cathode precharged and A electrolytes under high temperature (40 ℃): (a) CV windows at 30 mV s^{-1}, (b) CV plots at 10-160 mV s^{-1}, (c) GCD curves at 0.5-8 A g^{-1}, (d) rate performance, (e) Ragone behavior and (f) cycling behavior.

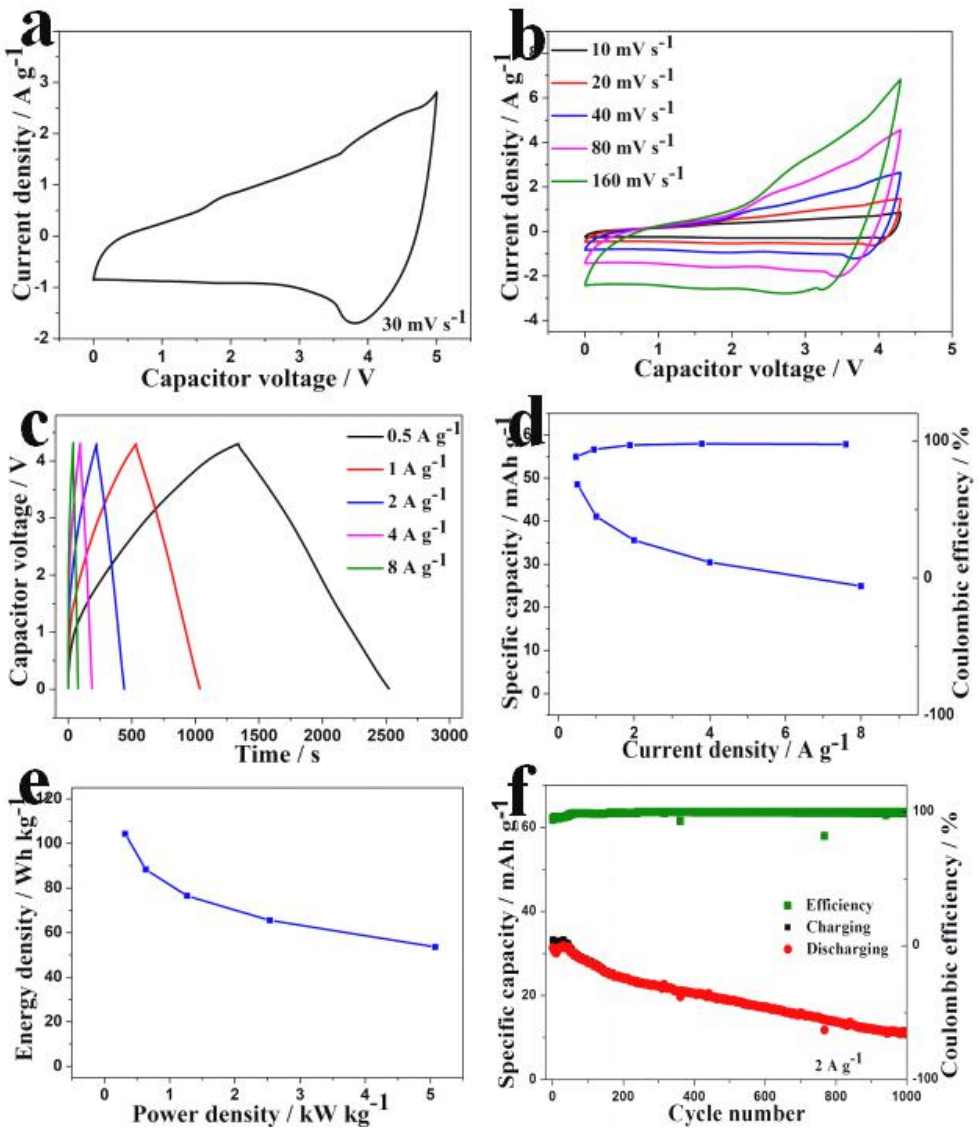

Fig. S62 Performance of KNCF (1-6)//918 DIB with the anode precharged and B electrolytes under high temperature (40 ℃): (a) CV windows at 10 mV s^{-1}, (b) CV plots at 10-160 mV s^{-1}, (c) GCD curves at 0.5-8 A g^{-1}, (d) rate performance, (e) Ragone behavior and (f) cycling behavior.

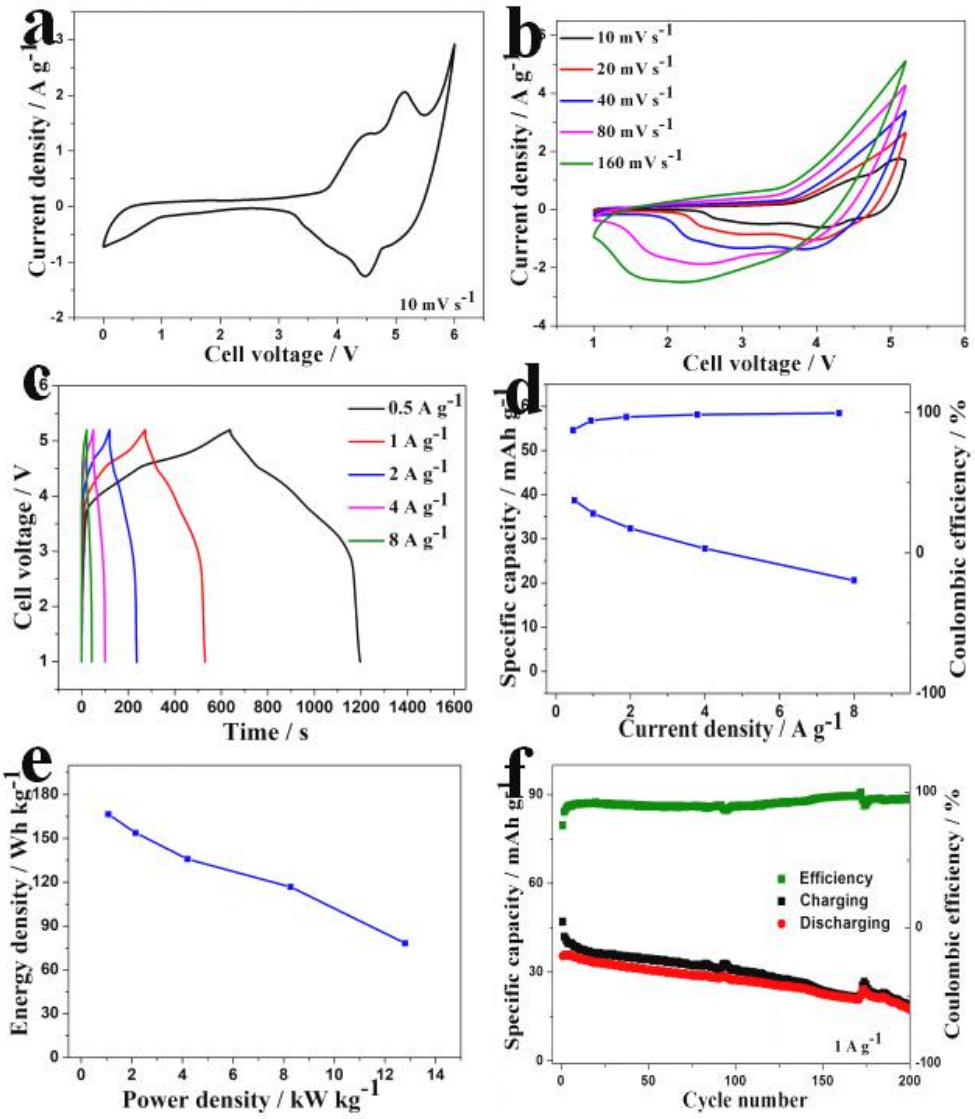

Table S1 The element analysis of KNCF (Ni/Co=1-6) sample by EDS and ICP methods

	Theoretical value		EDS		ICP	
Element	**Wt. %**	**At. %**	**Wt. %**	**At. %**	**Wt. %**	**At. %**
K	25.18	**20.00**	26.86	**21.61**	24.81	**19.72**
Ni	5.42	**2.86**	4.78	**2.56**	3.98	**2.10**
Co	32.59	**17.14**	33.29	**17.77**	34.49	**18.10**
F	36.81	**60.00**	35.07	**58.06**	36.82*	**60.07**
Molecular formula	$K_{1.0}Ni_{0.14}Co_{0.86}F_{3.0}$		$K_{1.1}Ni_{0.13}Co_{0.87}F_{2.9}$		$K_{1.0}Ni_{0.10}Co_{0.90}F_{3.0}$	

* Note: The content of F from ICP is caculated based on the total weight ratio of 100%.

Table S2 Specific capacity of the AC and KNCF electrodes (Ni/Co=1-0~0-1) with A electrolytes.

	Specific capacity / (mAh g^{-1})									
i / （A g^{-1}）	AC	KNCF electrodes (Ni/Co=1-0~0-1)								
		1-0	6-1	3-1	3-2	1-1	2-3	1-3	1-6	0-1
0.1	72.1	287.2	259.8	235.7	207.2	209.2	242.1	245.4	165.9	124.1
0.2	64.2	256.4	242.0	229.4	179.4	197.5	237.8	251.3	161.1	113.0
0.4	57.1	215.1	203.6	207.2	149.2	177.3	224.0	236.1	146.8	101.8
0.8	51.3	151.9	158.1	171.0	120.6	149.0	197.0	210.1	123.8	87.0
1.6	46.1	71.4	106.3	133.0	89.7	110.1	166.4	171.5	99.2	69.6
3.2	38.9	18.1	54.5	93.0	61.1	77.3	120.2	121.9	73.1	53.6

Table S3 The design of m_+/m_- ratios for KNCF (Ni/Co=1-0~0-1)//AC LICs with A electrolytes.

	The design of m_+/m_- ratios under different current densities for KNCF electrodes (Ni/Co=1-0~0-1)								
i / （A g^{-1}）	1-0	6-1	3-1	3-2	1-1	2-3	1-3	1-6	0-1
0.1	4.0	3.6	3.3	2.9	2.9	3.4	3.4	2.3	1.7
0.2	4.0	3.8	3.6	2.8	3.1	3.7	3.9	2.5	1.8
0.4	3.8	3.6	3.6	2.6	3.1	3.9	4.2	2.6	1.8
0.8	3.0	3.1	3.4	2.4	2.9	3.9	4.1	2.4	1.7
1.6	1.6	2.3	2.9	1.9	2.4	3.6	3.7	2.2	1.5
3.2	0.5	1.4	2.5	1.6	2.1	3.1	3.2	1.9	1.4
Average	**2.8**	**2.9**	**3.2**	**2.4**	**2.8**	**3.6**	**3.8**	**2.3**	**1.7**

Table S4 The design of m_+/m_- ratios for KNCF (1-6)//AC+LFP (1:1) LICs and KNCF (1-6)//AC+LFP (0:1) LIB with A electrolytes.

	Specific capacity / mAh g^{-1}			m_+/m_- ratio	
i **/ A g^{-1}**	**KNCF (1-6)**	**AC+LFP (1:1)**	**AC+LFP (0:1)**	**AC+LFP(1:1)/ KNCF(1-6)**	**AC+LFP(0:1) /KNCF(1-6)**
0.1	165.9	94.8	127.7	1.7	1.3:1
0.2	161.1	90.9	123.8	1.8	1.3:1
0.4	146.8	79.2	115.1	1.8	1.28:1
0.8	123.8	69.4	104.0	1.8	1.19:1
1.6	99.2	61.0	88.9	1.6	1.12:1
3.2	73.1	50.6	71.4	1.4	1.02:1
The designed value of m_+/m_- ratio				**1.7 (the average value)**	**1 (excess of KNCF (1-6) anode)**

Table S5 Specific capacity of graphite electrodes with A (918) and B (918, KS6, SAG) electrolytes, 918+AC (1:1), 918+LFP (1:1), 918+AC+LFP (1:1:1), KNCF (1-6) electrodes with B electrolytes.

	Specific capacity / mAh g^{-1}							
i **/（A g^{-1}）**	**918***	**918**	**KS6**	**SAG**	**918+AC**	**918+LFP**	**918+AC+LFP**	**KNCF(1-6)**
0.1	72	75	69	70	74	94	82	187
0.2	63	71	64	66	69	91	74	185
0.4	61	69	61	64	60	84	71	179
0.8	59	67	60	61	52	77	61	157
1.6	54	63	55	58	44	68	42	134
3.2	24	52	22	50	24	50	17	104

***Note:** the electrolytes for 918 electrode were A electrolytes, while the electrolytes for others in the table were B electrolytes.

Table S6 The design of m_+/m_- ratios for KNCF (1-6)//918, KNCF(1-6)//918+LFP (1:1), KNCF (1-6)//918+AC (1:1) and KNCF (1-6)//918+AC+LFP (1:1:1), KNCF (1-6)//SAG and KNCF (1-6)//KS6 DIBs with B electrolytes.

Li-DIBs or LIBs	m_+/m_- ratio
KNCF (1-6)//918	1:1
KNCF (1-6)//918+LFP (1:1)	1:1
KNCF (1-6)//918+AC (1:1)	1:1
KNCF (1-6)//918+AC+LFP (1:1:1)	1:1
KNCF (1-6)//SAG	1:1
KNCF (1-6)//KS6	1:1

Table S7 Performance summary of the LICs and DIBs in the study under room temperature: KNCF//AC LICs (1-0, 2-3, 1-6, 0-1) with the anode precharged at 0.5 A g^{-1}, KNCF(1-6)//AC+LFP(1:1) LIC with anode precharged at 0.5 A g^{-1}, Ni-Co(1-6)//AC LIC with both anode and cathode precharged at 0.5 A g^{-1} by using A electrolytes; KNCF(1-6)//918, KNCF(1-6)//918+AC(1:1), KNCF(1-6)//918+LFP(1:1) and KNCF(1-6)//918+AC+LFP(1:1:1) DIBs with anode precharged at 0.5 A g^{-1} by using B electrolytes.

Type	LICs / Li-DIBs / LIBs	Working voltage / V	Energy density / Wh kg^{-1}	Power density / kW kg^{-1}	Cycling behavior / retention%, repeated cycles, current density	
LICs	KNCF(1-0)//AC (1:2.8)	0.01-4.0	71-32.4-1.3	0.25-2-9.2	71%/3000/5A g^{-1}	60%/5000/5A g^{-1}
		0.01-4.3	86-42.4-6	0.27-2.2-6	70%/3000/5A g^{-1}	59%/5000/5A g^{-1}
		0.01-4.5	107-61-14	0.28-2.3-9	30%/1000/5A g^{-1}	23%/5000/5A g^{-1}
		0.01-4.7	130-71-17.4	0.3-2.3-9.5	29%/1000/5A g^{-1}	10%/5000/5A g^{-1}
	KNCF(0-1)//AC (1:1.7)	0.01-4.0	42-27-15	0.36-2.9-11.3	65%/1000/5A g^{-1}	45%/5000/5A g^{-1}
		0.01-4.3	60-31-5.1	0.36-3-11.5	60%/1000/5A g^{-1}	28%/5000/5A g^{-1}
		0.01-4.5	64-42-23	0.36-3.1-13	45%/1000/5A g^{-1}	31%/5000/5A g^{-1}
		0.01-4.7	74-44-20	0.43-3.4-12.7	53%/1000/5A g^{-1}	15%/5000/5A g^{-1}
	KNCF(1-6)//AC (1:2.3)	**0.01-4.0**	**61-37-15**	**0.3-2.4-9.5**	**119%/3000/5A g^{-1}**	**116%/5000/5A g^{-1}**
		0.01-4.3	**78-44-23**	**0.32-2.6-10.1**	**78%/3000/5A g^{-1}**	**70%/5000/5A g^{-1}**
		0.01-4.5	**96-46-11**	**0.33-2.6-10.5**	**64%/1000/5A g^{-1}**	35%/5000/5A g^{-1}
		0.01-4.7	**112-58-16**	**0.35-2.8-11.2**	**43%/1000/5A g^{-1}**	22%/5000/5A g^{-1}
	KNCF(1-6)//AC+LFP (1:1.7)	**0.01-4.0**	**95-61-27**	**0.37-3-11.8**	**82%/3000/5A g^{-1}**	**79%/5000/5A g^{-1}**
		0.01-4.3	**110-68-38**	**0.4-3.2-12.7**	**73%/1000/5A g^{-1}**	40%/5000/5A g^{-1}
		0.01-4.5	**129-75-31**	**0.42-3.4-12.6**	**79%/1000/5A g^{-1}**	33%/5000/5A g^{-1}
		0.01-4.7	**140-78-20**	**0.43-3.4-13.8**	**68%/1000/5A g^{-1}**	31%/5000/5A g^{-1}
	KNCF(1-6)//AC (1:2.3) (both electrodes precharged)	**0.01-4.0**	**73-46-20**	**0.3-2.4-9.6**	**97%/3000/5A g^{-1}**	**93%/5000/5A g^{-1}**
		0.01-4.3	**87-56-28**	**0.32-2.6-10.3**	**76%/3000/5A g^{-1}**	46%/5000/5A g^{-1}
		0.01-4.5	**104-61-27**	**0.34-2.7-10.8**	**72%/1500/5A g^{-1}**	33%/5000/5A g^{-1}
		0.01-4.7	**114-70-37**	**0.35-2.8-11.1**	**73%/1500/5A g^{-1}**	18%/5000/5A g^{-1}
DIBs	KNCF(1-6)//918 (1:1)	**0.5-5.2**	**152-118-46**	**0.9-3.4-10.4**	**74%/300/2A g^{-1}**	**69%/500/2A g^{-1}**
		0.5-5.5	**196-159-93**	**1-3.8-12.4**	**90%/100/2A g^{-1}**	**73%/200/2A g^{-1}**
	KNCF(1-6)//918+AC (1:1)	**0.5-5.2**	**104-76-29**	**0.58-2.3-9.4**	**69%/300/2A g^{-1}**	**64%/500/2A g^{-1}**
		0.5-5.5	**119-87-37**	**0.6-2.5-10**	**63%/100/2A g^{-1}**	36%/200/2A g^{-1}
	KNCF(1-6)//918+LFP (1:1)	**0.5-5.2**	**131-104-65**	**0.8-3-10.7**	**62%/300/2A g^{-1}**	46%/500/2A g^{-1}
		0.5-5.5	**167-134-54**	**0.8-3-9.4**	**77%/100/2A g^{-1}**	54%/200/2A g^{-1}
	KNCF(1-6)// 918+AC+LFP (1:1)	**0.5-5.2**	**107-84-43**	**0.6-2.4-9.4**	**79%/300/2A g^{-1}**	**66%/500/2A g^{-1}**
		0.5-5.5	**125-97-38**	**0.6-2.5-9.9**	**63%/100/2A g^{-1}**	39%/200/2A g^{-1}

Table S8 Performance summary of the LICs and DIBs in the study under high and low temperatures : KNCF(1-6)//AC, KNCF(1-6)//AC+LFP(1:1) LICs with the anode precharged at 0.5 A g^{-1}, KNCF(1-6)//AC LIC with both anode and cathode precharged at 0.5 A g^{-1} by using A electrolytes; KNCF(1-6)//918 DIBs with anode precharged at 0.5 A g^{-1} by using B electrolytes.

Type	LICs / Li-DIBs / LIBs	T / ℃	Voltage / V	Energy density / Wh kg^{-1}	Power density / kW kg^{-1}	Cycling behavior / retention%, repeated cycles, current density	
LICs	KNCF(1-6)//AC (1:2.3)	**-20**	**0.01-4.3**	**43.9-12.6**	**0.32-5.1**	**66%/500/2 A g^{-1}**	28%/5000/2 A g^{-1}
		40	**0.01-4.3**	**87.1-45.9**	**0.31-5.0**	**51%/500/2 A g^{-1}**	37%/1000/2 A g^{-1}
	KNCF(1-6)//AC+LFP (1:1.7)	**-20**	**0.01-4.3**	**26.4-3.5**	**0.38-6.3**	**71%/3000/2 A g^{-1}**	**68%/5000/2 A g^{-1}**
		40	**0.01-4.3**	**120-56**	**0.4-6.4**	**40%/500/2 A g^{-1}**	29%/1000/2 A g^{-1}
	KNCF(1-6)//AC (1:2.3) (both electrodes precharged)	**-20**	**0.01-4.3**	**30.6-6.9**	**0.31-5.0**	**60%/3000/2 A g^{-1}**	43%/5000/2A g^{-1}
		40	**0.01-4.3**	**104-54**	**0.32-5.1**	**61%/500/2 A g^{-1}**	35%/1000/2 A g^{-1}
DIBs	KNCF(1-6)//918 (1:1)	**-20**	**1-5.6**	**165-109-61**	**1.1-4.2-7.5**	**65%/500/1 A g^{-1}**	**43%/2000/1A g^{-1}**
		40	**1-5.2**	**166-116-78**	**1.1-8.3-12.8**	**78%/100/1 A g^{-1}**	**64%/150/1A g^{-1}**

Table S9 A comparison of this work with some advanced LICs

LICs	Working voltage / V	Energy density / Wh kg^{-1}	Power density / kW kg^{-1}	Cycling behavior / retention%, repeated cycles, current density	Refs.
CTAB-Sn(IV)@Ti_3C_2//AC	1.0-4.0	105.56-45.31	0.495-10.8	71.1%/4000/2 A g^{-1}	[1]
Fe_2O_3@C//N-HPC	1.0-4.0	65-31	0.368-9.2	84.1%/1000/1 A g^{-1}	[2]
$Li_4Ti_5O_{12}$/C//PGM	1.0-3.0	72-40	0.65-8.3	65%/1000/10 A g^{-1}	[3]
H-TiO_2/PPy/SWCNTs//AC	1.0-3.0	31.3-1.9	0.2-4.0	77.8%/3000/0.5 A g^{-1}	[4]
hp-LVO/C//CMK-3	0.2-4.3	105-62	0.188-9.3	71%/2000/1 A g^{-1}	[5]
$LiNi_{0.5}Mn_{1.5}O_4$//AC	1.5-3.25	19-8	0.13-3.5	81%/3000/1 A g^{-1}	[6]
100-LTO-G-600C//AC	1.5-3.0	52-12.8	0.225-57.6	97%/2000/25 A g^{-1}	[7]
Li_3VO_4//AC	1.0-4.0	136.4-24.4	0.532-11.02	87%/1500/2 A g^{-1}	[8]
MnNCN//AC	0.1-4.0	103-10	0.14-8.533	100%/5000/5 A g^{-1}	[9]
TiO_2 NBA// graphene hydrogels	0.0-3.8	82-21	0.57-19	73%/600/1 A g^{-1}	[10]
TiO_2@EEG//EEG	0.0-3.0	72-10	0.303-2.0	68%/1000/1.5 A g^{-1}	[11]
3D HTO NWAs//AC	0.0-3.0	93.8-33.3	0.3-15	78.8%/3000/5 A g^{-1}	[12]
SnO_2-C//C	0.5-4.0	110-49	0.19-2.96	80%/2000/1 A g^{-1}	[13]
KNCF(1-6)//AC+LFP (1:1.7)	**0.01-4.0**	**95-61-27**	**0.37-3-11.8**	**82%/3000/5 A g^{-1} 79%/5000/5 A g^{-1}**	**This work**
	0.01-4.3	**110-68-38**	**0.4-3.2-12.7**	**73%/1000/5 A g^{-1}**	
	0.01-4.5	**129-75-31**	**0.42-3.4-12.6**	**79%/1000/5 A g^{-1}**	
	0.01-4.7	**140-78-20**	**0.43-3.4-13.8**	**68%/1000/5 A g^{-1}**	
KNCF(1-6)//AC (1:2.3) (both electrodes precharged)	**0.01-4.0**	**73-46-20**	**0.3-2.4-9.6**	**97%/3000/5 A g^{-1} 93%/5000/5 A g^{-1}**	
	0.01-4.3	**87-56-28**	**0.32-2.6-10.3**	**76%/3000/5 A g^{-1}**	
	0.01-4.5	**104-61-27**	**0.34-2.7-10.8**	**72%/1500/5 A g^{-1}**	
	0.01-4.7	**114-70-37**	**0.35-2.8-11.1**	**73%/1500/5 A g^{-1}**	

Table S10 A comparison of this work with some advanced DIBs

DIBs	Working voltage / V	Energy density / Wh kg^{-1}	Power density / kW kg^{-1}	Cycling behavior / retention%, repeated cycles, current density	Refs.
Graphite//Graphite	0.01-5.2	108 (0.05 A g^{-1})	/	67%/50/0.05 A g^{-1}	[14]
Li//Graphite	3.4-5.0	220 (0.05 A g^{-1})	/	71%/500/0.05 A g^{-1}	[15]
Al//graphite	3.0-5.0	222-150	0.132-1.2	88%/200/0.2 A g^{-1}	[16]
ME-DIB (3D Al//graphite)	3.0-4.95	206-158	0.166-1.758	92.4%/1000/0.2 A g^{-1}	[17]
Graphite (MTI)//KS6	3.0-5.1	125-25	0.4-0.5	200/90%/0.5 A g^{-1}	[18]
TiO_2//Graphite	1.5-3.7	36 (0.1 Ag^{-1})		88.6%/50/0.1 A g^{-1}	[19]
Nb_2O_5//Graphite	1.5-3.5	52 (0.1 Ag^{-1})	/	85%/50/0.1 A g^{-1}	[20]
MoO_3//KS6	1.5-3.5	77 (0.1 Ag^{-1})	/	90%/200/0.1 A g^{-1}	[21]
2D Si//Graphite	0-3.5	54 (0.1 Ag^{-1}) 40 ℃	/	61%/100/0.1 A g^{-1}	[22]
KNCF(1-6)//918 (1:1)	**0.5-5.2**	**152-118-46** (0.5-2-8 A g^{-1})	**0.9-3.4-10.4** (0.5-2-8 A g^{-1})	**74%/300/2A g^{-1} 69%/500/2A g^{-1}**	**This work**
	0.5-5.5	**196-159-93** (0.5-2-8 A g^{-1})	**1-3.8-12.4** (0.5-2-8 A g^{-1})	**90%/100/2A g^{-1} 73%/200/2A g^{-1}**	
KNCF(1-6)//918+AC (1:1)	**0.5-5.2**	**104-76-29** (0.5-2-8 A g^{-1})	**0.58-2.3-9.4** (0.5-2-8 A g^{-1})	**69%/300/2A g^{-1} 64%/500/2A g^{-1}**	
	0.5-5.5	**119-87-37** (0.5-2-8 A g^{-1})	**0.6-2.5-10** (0.5-2-8 A g^{-1})	**63%/100/2A g^{-1}**	
KNCF(1-6)//918+LFP (1:1)	**0.5-5.2**	**131-104-65** (0.5-2-8 A g^{-1})	**0.8-3-10.7** (0.5-2-8 A g^{-1})	**62%/300/2A g^{-1}**	
	0.5-5.5	**167-134-54** (0.5-2-8 A g^{-1})	**0.8-3-9.4** (0.5-2-8 A g^{-1})	**77%/100/2A g^{-1}**	
KNCF(1-6)// 918+AC+LFP (1:1)	**0.5-5.2**	**107-84-43** (0.5-2-8 A g^{-1})	**0.6-2.4-9.4** (0.5-2-8 A g^{-1})	**79%/300/2A g^{-1} 66%/500/2A g^{-1}**	
	0.5-5.5	**125-97-38** (0.5-2-8 A g^{-1})	**0.6-2.5-9.9** (0.5-2-8 A g^{-1})	**63%/100/2A g^{-1}**	

Table S11 Chemicals, agents and materials used in this study

Chemials, Agents and Materials	Type or level	Company	Detailed characteristics or parameters
$NiCl_2$•$6H_2O$	AR	SinoPharm	purity≥98.0%
$CoCl_2$•$6H_2O$	AR	SinoPharm	purity≥99.0%
KF•$2H_2O$	AR	SinoPharm	purity≥99.0%
PVP-K30	GR	SinoPharm	K value (%): 27.4-32.0; N (%): 11.5~12.8
EG	AR	SinoPharm	purity≥99.0%
NMP	AR	SinoPharm	purity≥99.0%
AB	Battery grade	/	/
PVDF	Battery grade	/	/
Li plate	15.6*0.45 mm	China Energy	15.6*0.45 mm
Cu foil	200*0.015	GuangZhou JiaYuan	Total thickness: 15 μm; weight: 87 g m^{-2}
Carbon coated-Al foil	222*0.015	GuagZhou NaNuo	Total thickness: 17 μm; Strength: 192 Mpa
Glass microfiber filters	GF/D 2.7 μm; 1823-025	Whatman	Diameter: 25 mm; Thickness: 675 μm; weight: 121 g m^{-2}
AC	YEC 8b	FuZhou YiHuan	D50: ~10 μm; Density: 0.4 g cm^{-3}; SSA:2000~2500 m^2 g^{-1}
Graphite	918	BTR	D50: 17-20 μm; Tab: 0.95-1.2 g cm^{-3}; SSA:3.0-4.0 m^2 g^{-1}
Graphite	SAG	BTR	D50: 19.0 ± 1.5 μm; Tab: 0.9 ± 0.1 g cm^{-3}; SSA:3.3 ± 0.5 m^2 g^{-1}
Graphite	KS6	TiMCAL	D90: 5.8-7.1 μm; Interlayer distance: 0.3354-0.3360 nm; SSA: 20 m^2 g^{-1}; Density-Scott: 0.07 g cm^{-3};
$LiFePO_4$	LFP-NCO	Aleees	D50: 4 ± 2 μm; Tab: 1 ± 0.2 g cm^{-3}; SSA:13 ± 2 m^2 g^{-1}
A electrolytes	LBC-305-01	CAPCHEM	1 M $LiPF_6$/EC:EMC:DMC (1:1:1) /1% VC
B electrolytes	LBC-3045I	CAPCHEM	1 M $LiPF_6$/EC:EMC:DEC (1:1:1)/ FEC,etc.
Cell components	CR-2032	ShenZhen TianChenHe	/

Methods: Calculations for m_+/m_-, C_m, E_m, P_m

The mass ratios of positive and negative active materials for the LICs at various current densities were calculated based on the charge-balance ($Q+ = Q-$), as shown in equation (1). The specific capacity (C_m, mAh g^{-1}), energy density (E_m, Wh kg^{-1}) for LICs, energy density (E_m, Wh kg^{-1}) for Li-DIBs and LIBs, and power density (P_m, kW kg^{-1}) were calculated according to the equations (2), (3), (4) and (5).

$$\boldsymbol{m_+/m_- = Q_{m-}/Q_{m+}} \quad \textbf{(1)}$$

$$\boldsymbol{C_m = Q_m / 3.6 = I\,t / 3.6\,m} \quad \textbf{(2)}$$

$$\boldsymbol{E_m\ (Capacitor) = (C_m \triangle V) / 2} \quad \textbf{(3)}$$

$$\boldsymbol{E_m\ (Battery) = (C_m V)} \quad \textbf{(4)}$$

$$\boldsymbol{P_m = 3.6\,E_m / t_d} \quad \textbf{(5)}$$

Where m, Q_m, $\triangle V$, V, I and t refer to the mass of active materials (g) (for half cells, it means the mass of active materials of anode or cathode; for full cells, it means the total masses of active materials of anode and cathode), specific charge quantity (C g^{-1}), potential window (V), potential of the discharging plateaus (V), current (A) and charging or discharging time (s) (for anode, it means the charging time; for cathode and full cells, it refers to the discharging time), respectively.

The references in the Tables S9-10:

[1] J. M. Luo, W. K. Zhang, H. D. Yuan, C. B. Jin, L. Y. Zhang, H. Huang, C. Liang,Y. Xia, J. Zhang, Y. P. Gan and X. Y. Tao, Pillared structure design of mxene with ultralarge interlayer spacing for high-performance lithium-ion capacitors, *ACS Nano*, 2017, **11**, 2459-2469.

[2] X. L. Yu, J. J. Deng, C. Z. Zhan, R. T. Lv, Z. H. Huang, F. Y. Kang, A high-power lithium-ion hybrid electrochemical capacitor based on citrate-derived electrodes, *Electrochim. Act*a, 2017, **228**, 76-81.

[3] L. Ye, Q. H. Liang, Y. Lei, X. L. Yu, C. P. Han, W. C. Shen, Z. H. Huang, F. Y. Kang, Q.-H. Yang, A high performance li-ion capacitor constructed with li4ti5o12/c hybrid and porous graphene macroform. *J. Power Sources*, 2015, **282**, 174-178.

[4] G. Tang, L. J. Cao, P. Xiao, Y. H. Zhang, H. Liu, A novel high energy hybrid li-ion capacitor with a three-dimensional hierarchical ternary nanostructure of hydrogen-treated TiO_2 nanoparticles/conductive polymer/carbon nanotubes anode and an activated carbon cathode, *J. Power Sources*, 2017, **355**, 1-7.

[5] X. N. Xu, F. E. Niu, D. P. Zhang, C. X. Chu, C. S. Wang, J. Yang, Y. T. Qian, Hierarchically porous Li_3VO_4/C nanocomposite as an advanced anode material for high-performance lithium-ion capacitors, *J. Power Sources*, 2018, **384**, 240-248.

[6] H.-K. Kim, D. Mhamane, M.-S. Kim, H.-K. Roh, V. Aravindan, S. Madhavi, K. C. Roh, K.-B. Kim, Nanostructured spinel $LiNi_{0.5}Mn_{1.5}O_4$ as new insertion anode for advanced li-ion capacitors with high power capability, *Nano Energy*, 2015, **12**, 69-75.

[7] G. K. Wang, C. X. Lu, X. Zhang, B. Wan, H. Y. Liu, M. R. Xia, H. Y. Gou, G. Q. Xin, J. Lian, Y. G. Zhang, Toward ultrafast lithium ion capacitors: a novel atomic layer deposition seeded preparation of $Li_4Ti_5O_{12}$/graphene anode, *Nano Energy*, 2017, **36**, 46-57.

[8] L. F. Shen, H. F. Lv, S. Q. Chen, P. Kopold, P. A. van Aken, X. J. Wu, J. Maier and Y. Yu, Peapod-like Li_3VO_4/N-doped carbon nanowires with pseudocapacitive properties as advanced materials for high-energy lithium-ion capacitors, *Adv. Mater.*, 2017, **29**, 1700142.

[9] C. F. Liu, C. K. Zhang, H. Y. Fu, X. H. Nan and G. Z. Cao, Exploiting high-performance anode through tuning the character of chemical bonds for li-ion batteries and capacitors, *Adv. Energy Mater.*, 2017, **7**, 1601127.

[10] H. W. Wang, C. Guan, X. F. Wang and H. J. Fan, A high energy and power li-ion capacitor based on a TiO_2 nanobelt array anode and a graphene hydrogel cathode. *Small*, 2015, 11, 1470-1477.

[11] F. X. Wang, C. Wang, Y. J. Zhao, Z. C. Liu, Z. Chang, L. J. Fu, Y. S. Zhu, Y. P. Wu and D. Y. Zhao, A quasi-solid-state li-ion capacitor based on porous TiO_2 hollow microspheres wrapped with graphene nanosheets. *Small*, 2016, **12**, 6207.

[12] L. F. Que, Z. B. Wang, F. D. Yu and D. M. G, 3D ultralong nanowire arrays with a tailored hydrogen titanate phase as binder-free anodes for Li-ion capacitors, *J. Mater. Chem. A*, 2016, **4**, 8716-8723.

[13] W.-H. Qu, F. Han, A.-H. Lu, C. Xing, M. Qiao and W.-C. Li, Combination of a SnO_2 – C hybrid anode and a tubular mesoporous carbon cathode in a high energy density non-aqueous lithium ion capacitor: preparation and characterisation, *J. Mater. Chem. A*, 2014, **2**, 6549

[14] J. A. Read, A. V. Cresce, M. H. Ervin and K. Xu, Dual-graphite chemistry enabled by a high voltage electrolyte. *Energy Environ. Sci.*, 2014, **7**, 617-620.

[15] P. Meister, V. Siozios, J. Reiter, S. Klamor, S. Rothermel, O. Fromm, H.-W. Meyer, M. Winter and T. Placke, Dual-ion cells based on the electrochemical intercalation of asymmetric fluorosulfonyl-(trifluoromethanesulfonyl) imide anions into graphite, *Electrochim. Acta*, 2014, **130**, 625-633.

[16] X. L. Zhang, Y. B. Tang, F. Zhang and C.-S. Lee, A Novel Aluminum-Graphite Dual-Ion Battery, *Adv. Energy. Mater.*, 2016, **6**, 1502588.

[17] S. Q. Zhang, M. Wang, Z. M. Zhou and Y. B. Tang, Multifunctional Electrode Design Consisting of 3D Porous Separator Modulated with Patterned Anode for High-Performance Dual-Ion Batteries, *Adv. Funct. Mater.*, 2017, **27**, 1703035.

[18] C. Y. Chan, P.-K. Lee, Z. H. Xu and D. Y. W. Yu, Designing high-power graphite-based dual-ion batteries, *Electrochim. Acta*, 2018, **263**, 34-39.

[19] A. K. Thapa, G. Park, H. Nakamura, T. Ishihara, N. Moriyama, T. Kawamura, H. Y. Wang and M. Yoshio, Novel graphite/TiO_2 electrochemical cells as a safe electric energy storage system, *Electrochim. Acta*, 2010, **55**, 7305-7309.

[20] G. Park, N. Gunawardhana, C. Lee, S. M. Lee, Y. S. Lee and M. Yoshio, Development of a novel and safer energy storage system using a graphite cathode and Nb_2O_5 anode, *J. Power Sources,* 2013, **236**, 145-150.

[21] N. Gunawardhana, G. J. Park, N. Dimov, A. K. Thapa, H. Nakamura, H. Y. Wang, T. Ishihara and M. Yoshio, Constructing a novel and safer energy storing system using a graphite cathode and a MoO_3 anode, J. Power Sources, 2011, **196**, 7886-7890.

[22] H. Nakano, Y. Sugiyama, T. Morishita, M. J. S. Spencer, I. K. Snook, Y. Kumai and H. Okamoto, Anion secondary batteries utilizing a reversible BF_4 insertion/extraction two-dimensional Si material, *J. Mater. Chem. A*, 2014, **2**, 7588-7592.